*sustainability*

MDPI

*Article*

# Green Roofs as a Nature-Based Solution to Mitigate Urban Heating During a Heatwave Event in the City of Athens, Greece

**Christos Spyrou [1,*], Marika Koukoula [2], Pantelis-Manolis Saviolakis [3], Christos Zerefos [1,4,5,6], Michael Loupis [7,8], Charis Masouras [7,8], Aikaterini Pappa [3] and Petros Katsafados [3]**

[1] Research Centre for Atmospheric Physics and Climatology, Academy of Athens, 10679 Athens, Greece; zerefos@geol.uoa.gr
[2] Institute of Earth Surface Dynamics, University of Lausanne, 1015 Lausanne, Switzerland; marika.koukoula@unil.ch
[3] Department of Geography, Harokopio University of Athens (HUA), 17671 Athens, Greece; saviolakis@hua.gr (P.-M.S.); pkatsaf@hua.gr (P.K.)
[4] Biomedical Research Foundation of the Academy of Athens, 11527 Athens, Greece
[5] Navarino Environmental Observatory (N.E.O.), Costa Navarino, 24001 Messinia, Greece
[6] Mariolopoulos-Kanaginis Foundation for the Environmental Sciences, 10675 Athens, Greece
[7] General Department, National and Kapodistrian University of Athens, 34400 Psachna, Greece; mloupis@itcnet.gr (M.L.); charismasouras@itcnet.gr (C.M.)
[8] Innovative Technologies Centre S.A. (ITC), 11633 Athens, Greece
* Correspondence: cspyrou@academyofathens.gr

**Abstract:** This study investigates the impact of green roof (GR) implementations as a mitigation strategy for urban heating during an extreme heat wave event in Athens, Greece, from 28 July to 5 August 2021. Three GR scenarios were simulated, namely 100% grass coverage, 100% sedum coverage, and 50% grass coverage, using the Weather Research and Forecasting model (WRF) in conjunction with the multi-layer urban-canopy-model BEP&BEM (Building Effect Parameterization/Building Energy Model) and extra urban land-use categories from Local Climate Zones (LCZ). Based on the results, GRs alter the local heat balance in the Greater Area of Athens (GAA), leading to a total temperature reduction. The 100% grass coverage proved to be the most effective, particularly during daytime, reducing the 2 m temperature field by approximately 0.7 °C (mean value) in the GAA. In some locations, temperature reductions exceeded 2 °C, depending on the local characteristics and the direction of the prevailing winds. Grass offered superior cooling effects compared to sedum, although sedum is more resilient to dry and moderate climates. The extent of vegetation coverage played an important role in the effectiveness of GRs. Reducing the coverage by 50% significantly reduced the cooling benefits, highlighting the importance of maximizing vegetation coverage to achieve notable temperature reductions.

**Keywords:** green roofs; urban heat island effect; nature-based solutions; urban modelling; heatwaves; climate change mitigation

check for updates

**Citation:** Spyrou, C.; Koukoula, M.; Saviolakis, P.-M.; Zerefos, C.; Loupis, M.; Masouras, C.; Pappa, A.; Katsafados, P. Green Roofs as a Nature-Based Solution to Mitigate Urban Heating During a Heatwave Event in the City of Athens, Greece. *Sustainability* **2024**, *16*, 9729. https://doi.org/10.3390/su16229729

Academic Editor: Adriana Del Borghi

Received: 7 October 2024
Revised: 1 November 2024
Accepted: 4 November 2024
Published: 8 November 2024

**Copyright:** © 2024 by the authors. Licensee MDPI, Basel, Switzerland. This article is an open access article distributed under the terms and conditions of the Creative Commons Attribution (CC BY) license (https://creativecommons.org/licenses/by/4.0/).

## 1. Introduction

One of the most important anthropogenic problems of modern cities, especially during hot periods, is the urban heat island (UHI) effect [1]. The UHI constitutes a distinct urban climate that is characterized by higher temperatures over densely built-up areas compared to the surrounding rural or less populated ones [2]. UHIs can be considered as an example of a local climate change. The main cause of the UHI is urban development. As the urban population increases, cities expand and densify. The natural landscape is being replaced by non-reflective construction materials with low albedo and increased thermal capacity, while tall buildings and narrow street canyons trap the incoming solar radiation, increasing the heat storage of the city, with consequent elevation of the ambient temperature and a strengthening of the UHI effect. Furthermore, human activity is responsible for the

production of excess heat through the cooling of buildings, transportation, etc. [3,4]. As a result, the rising temperatures in city centers associated with the heat island phenomenon have a negative impact both in human health and in the environment due to the increased heat exposure and energy demand for cooling [5].

In mid-latitudes, the synergistic effect between heat waves (HWs) and UHI is of great importance, especially under the framework of the global climate change that is responsible for more frequent, severe, and longer-lasting extreme HW events [6,7]. Based on the future projections, the increase in the mean global temperature and the expected more frequent and prolonged HWs will strengthen the associated heat island intensity affecting the extreme heat conditions of the urban areas [8,9]. Under these considerations, urban planning aims at finding solutions to mitigate these effects.

Mitigations strategies intend to improve the thermal comfort of the population and reduce the energy consumption for the cooling of buildings. The European Commission has addressed nature-based solutions as cost-effective and beneficial for the resilience of the environment solutions that can be easily applied to cities by increasing green spaces to achieve the sustainable development goals. Given though that the unbuilt areas in an urban city are limited, roofs have great potential since their extensive percentage of coverage in an urban city can provide a great alternative in hosting natural greenery [5,10,11]. Green or living roofs either fully or partially covered by vegetation can substantially alter the local heat balance equation [12], playing the role of a cooling mechanism by increasing the latent heat flux (through evapotranspiration) and thus reducing the sensible heat flux. In general, the extra heat stored in the urban region compared to the rural region in its vicinity causes the UHI phenomenon that stems from the extra anthropogenic heat flux, the difference in absorbance/emissivity of the incoming radiation, and the differences in the surface latent/sensible heat fluxes [13–17]. GRs mostly affect the development of the daytime boundary layer and have minimal impact on nighttime temperatures [14]. Compared to conventional roofs, they can reduce the energy demand of buildings for cooling [5,18]. Their cooling effectiveness can vary significantly based on the vegetation type, such as grass, shrubs, and trees [19], and the rooftop coverage [14,20]. Ref. [21] showed that the green roof fraction and the UHI reduction are linearly associated. Ref. [22] studied the cooling effect of GRs in four cities, each with varying urban density and distinct climate characteristics: Cairo (hot-dry), Hong Kong (hot-humid), Tokyo (warm-humid), and Paris (temperate). The results showed a temperature reduction during daytime that ranged between 0.1° and 0.6° and an increase in temperature of about 0.2° during the night.

Ref. [23], based on a study performed over mega-cities located in different climate zones within the United States, showed that UHI mitigation strategies have different results depending on the region, signifying the need for strategies tailored to the local climatic characteristics of the studied area. A recent review on the cooling potential of GRs [24] compared the results from 89 studies conducted in areas of different climatic categories and concluded that GRs perform better in dry climates than in hot and humid climates, but in both cases, the temperature reduction could exceed 1 °C. Ref. [25] conducted a study to assess the seasonal effect of GRs in the city of Porto, which is characterized by a mixed temperate oceanic and Mediterranean climate. They concluded that GRs reduced the 2 m temperature in summer and spring months and increased the 2 m temperature in winter and autumn months with a magnitude of 1 °C. The geographic location of the city, the topography of the area, the weather conditions (winds and clouds), the time of the day, the season of the year, and the city size and formation are factors that affect the spatio-temporal characteristics and the intensity of the UHI. For instance, coastal cities or cities located near large bodies of water benefit from a cooling effect due to thermal circulations generated by the differential heating of water and land that convects heat away from cities [26]. The intensity of this phenomenon and the resulting local air circulations are closely linked to the time of day and the season. Additionally, topography can influence heat island formation by either blocking winds from reaching the city or creating distinct wind patterns that can pass through it. In mid-latitude cities, heat islands are typically most intense during the

summer or winter seasons, especially at night. Regarding the city formation, cities that are mostly covered by elevated buildings that act as obstacles will result in a wind speed reduction and an increase of UHI effect [27]. Thus, UHI intensity and extent is affected by several complex mechanisms that need to be accurately understood before mitigation solutions are proposed.

To this end, ref. [28] made a thorough analysis of the governing mechanisms that force the UHI effect over the city of Athens, through the study of an Urban Heat Exposure (UHeatEx) indicator that takes into consideration the complexity of the city in three dimensions, the turbulent energy exchanges as expressed through sensible and latent heat flux, and the anthropogenic heat emissions (either from vehicles or heating/cooling). For their analysis, they adopted the LCZ land-use categorization. They found a high canyon aspect ratio and high Bowen ratio due to limited green spaces and high anthropogenic heat emissions, thus concluding that Athens is highly vulnerable to the UHI effect and the ramifications of climate change. Therefore, Athens has been selected among various studies conducted recently as an indicative region to evaluate mitigation strategies of the continuously observed urban overheating and UHI effect [29,30]. These studies have concluded that GRs are a promising solution to leverage climate change in urban areas. This is a common finding of similar research carried out in dense cities worldwide and in the vicinity of Athens, like Rome [31], Lisbon [32], and Ankara [33]. All in all, the literature underlines that GRs can be effectively used to increase green spaces in dense urban cities and that they have the potential to become significant climate change mitigators.

The scope of this study is to assess the heat island mitigation potential of GRs in the city of Athens (Greece) during an extreme prolonged HW episode that initiated in late July 2021. The study region is of scientific interest due to its complex and distinctive geomorphology, as it is a coastal region surrounded by mountains, and it is highly affected by HWs. It is anticipated that HWs will become more frequent and more powerful in the immediate future [34], so it is imperative to study the performance of GR in such meteorological events, which cause thousands of mortalities each year in Europe (U-shaped relationship [35]) and increase the health vulnerability of urban residents [36]. Undoubtedly, Athens belongs to the top-ranked European cities that will be impacted by climate change in heat-related issues [37–39]. According to the authors' knowledge, only one study has been conducted for Athens that assessed the impact of urban heating mitigation scenarios during HW conditions. The findings indicated a reduction in temperature up to 0.2° during daytime, a decrease in wind speed of about 0.5–1 m/s, and a smaller inland penetration of the sea breeze (SB) along its axis [40].

In the present study, to represent the GR effect inside the complex urban environment, an advanced numerical modeling approach along with a detailed description of the urban landscape were used. In particular, the modeling system utilized for this study consists of the state-of-the-art mesoscale Weather Research and Forecasting model (WRF v4.3.3) coupled with the advanced multilayer urban canopy scheme BEP/BEM (Building Effect Parameterization/Building Energy Model) [41,42]. The latter incorporates a land-surface scheme for GRs. The selected system (WRF coupled with BEP/BEM) has been evaluated for its performance in several studies across various regions and is considered a suitable tool for describing the urban meteorological conditions [43–45]. Based on the literature, there are a plethora of other sophisticated methods that can be used for modeling the building energy impact on the urban environment, but it was the scope of each study that determined which method was more appropriate. As described by [46], urban canopy parameterizations coupled with mesoscale numerical models result in more realistic simulations when the latter exceeds the building scale, where other methods such as EnergyPlus and TRNYS perform well. This supremacy of the urban canopy parameterizations with numerical models stems from their ability to build a physical-based framework in which the simulation is regulated by the continuous interactions between the neighboring buildings and the surrounding atmospheric conditions, especially in a densely built city like Athens. To accurately describe the morphology of Athens and use the full capabilities of

such an advanced urban canopy scheme, a detailed map based on LCZ classification has been utilized [28,47]. The LCZ classification has been successfully used in several urban climate studies over Europe [48–52]. However, the publicly available LCZ map for Athens, which was derived under the framework of the World Urban Database and Access Portal Tools (WUDAPT) project in its original form, is inherently generic in order to be universally applicable and cannot capture the specific characteristics of an urban or rural site [1]. For this reason, the tailored map used in the present study provides a more accurate alternative. This dataset was utilized by [28] to study the thermal environment of Athens and by [47] to perform an atmospheric and human–biometeorological analysis for Athens during the HW of July–August 2021.

In this paper, for the first time, different GR scenarios in terms of vegetation type and roof coverage were applied in the area of Athens and evaluated for their impact on the UHI effect during an extreme HW event. The modeling configuration used (WRF model–urban scheme BEP/BEM–land-surface model for GRs) is considered the most advanced system to assess this kind of processes, and this is the first time that it was used in conjunction with the detailed urban land-cover map (LCZ-CLIMPACT) that was exclusively produced for the area of Athens.

In the following sections, a detailed description of the study area, the synoptic conditions, and the adopted methodology are given, followed by the synoptic and mesoscale analysis of the HW and a discussion of the main outcomes of this study. The Conclusions Section summarizes the main findings of this work.

## 2. Study Area—Synoptic Conditions

The study region is the Greater Area of Athens (GAA), the capital city of Greece. It covers an area of 361 $km^2$, consists of 40 municipalities, and can be divided into five regional units (North, South, West, and East Athens and Piraeus) based on geographical criteria. It is a densely built-up coastal city located in the eastern Mediterranean. It features a complex and unique geomorphology, as it is a coastal region bordered by mountains to the west-northwest and east-northeast (Figure 1). HW events are common during the summer months, particularly in July and August. The area is also known for its UHI effect, which, in the hot-dry summer months, becomes more intense, reaching maximum values during daytime [7]. The prevailing conditions over the area during the warm period are formed either by the local thermal circulations, including SB and UHI circulation, or by the N-NE synoptic winds (Etesians), depending on the strength of the latter. Strong northerly winds can block the penetration of the SB into the mainland, while the weakening of the Etesians allows the development of SB and the local thermally induced UHI circulation [53].

To assess the effect of GRs on urban heating, a prolonged HW event was selected. It started on 28 July 2021 and lasted until 5 August 2021. This event was one of the strongest HWs in Greece in the last decade, with exceptionally high temperatures. During this period, strong anticyclonic conditions prevailed over the Eastern Mediterranean (Figure 2a), accompanied by a strong ridge mainly originating from SW, over Libya, and extended NE, affecting Greece and Turkey. This long-lasting system (10 days) transferred very hot and dry air masses to the area, with 850 hPa advected temperatures exceeding 300 K (approx. 27 °C) on 3 August 2021. A local minimum of 700 hPa specific humidity was also spotted in southern Greece, while the prevailing atmospheric circulation favored moisture advection over the Tyrrhenian and Adriatic Sea (Figure 2b). The combination of the anticyclone with the thermal low over the Anatolian Peninsula and the Middle East triggered the development of a strong flow varying from northeast to northwest directions over the Aegean Sea (Etesians winds). Etesians are strong and dry northern winds blowing at the interface of the two systems, and this is a typical summer circulation pattern in the area [54]. The strong synoptic flow over the Aegean Sea, which exceeded 10 $m \cdot s^{-1}$ (Figure 2c), interacted with mesoscale circulations, such as sea, mountain, and valley breezes, and produced complex local-scale flows over the Attica Basin, therefore affecting the intensity and the duration of Athens' UHI.

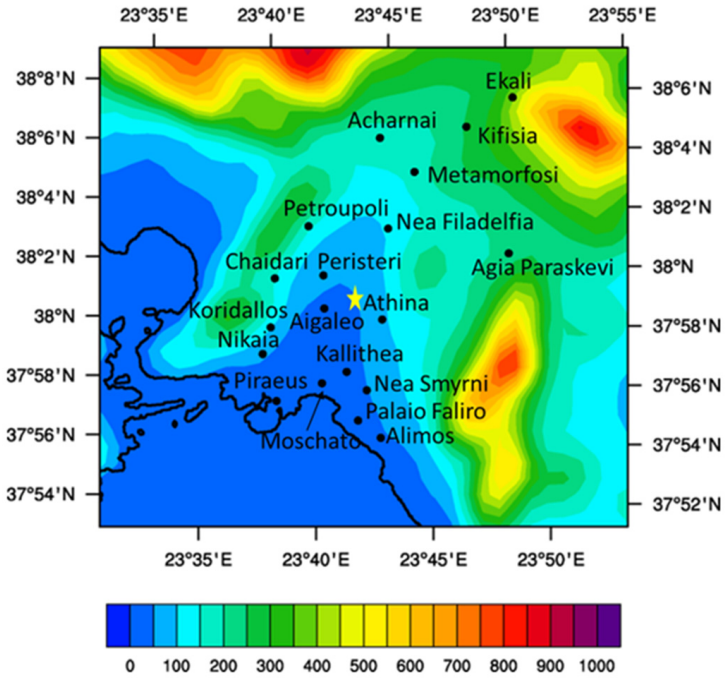


**Figure 1.** Topographic map (m) of the Attica prefecture showing the location of Athens' city center (Athina), along with stations at Harokopio University of Athens (Kallithea), Agia Paraskevi, and several other suburbs of the GAA.

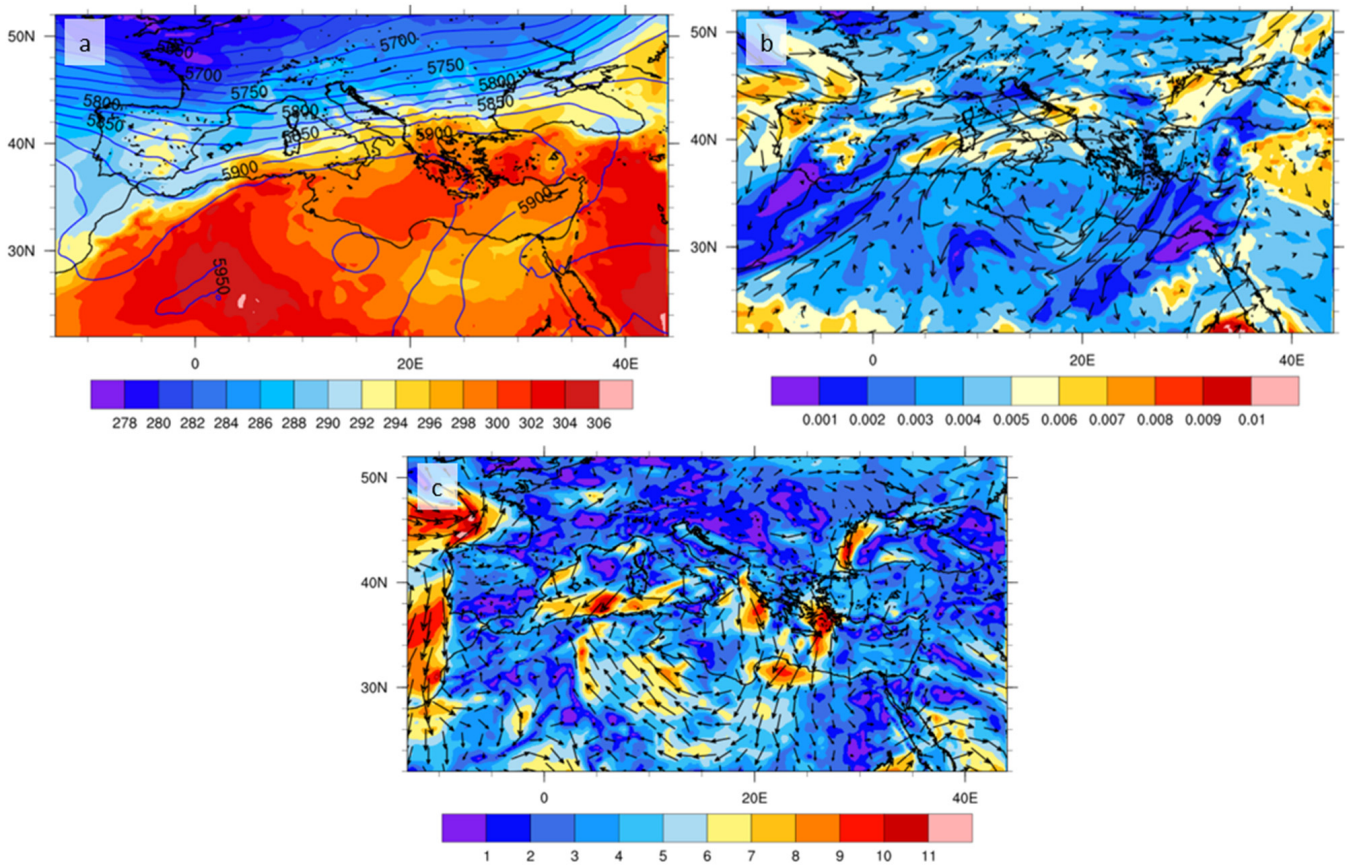


**Figure 2.** (**a**) Temperature at 850 hPa (K) and geopotential height at 500 hPa (m); (**b**) specific humidity (kg/kg) and wind vectors at 700 hPa; (**c**) wind speed and direction at 10 m (m $s^{-1}$) on 3 August 2021 at 12 UTC (Source Copernicus ERA5 Reanalysis).

The most prominent feature of the heatwave was the prolonged elevated temperatures throughout the day, especially during nighttime, which, in combination with the UHI effect, led to extreme heat conditions in the city of Athens. The National Observatory of Athens (NOA) recorded a daily minimum of 31.6 °C and a mean temperature of 36.5 °C. These values are the highest ever recorded at NOA [55]. The HW of 2021 was found to be the longest ever recorded at NOA (since the mid-19th century), with a total duration of 10 days. The maximum temperature of the hottest day (3 August 2021) was 43.9 °C, the second-highest temperature ever recorded at NOA. The highest was 44.8 °C, and it was recorded on 26 June 2007 [56].

## 3. Materials and Methods

### *3.1. Green Roofs Categorization*

In this study, GRs are proposed as a nature-based solution to mitigate excessive urban heating in the GAA during a HW period. Depending on the plant properties and usage, GRs can be classified as either intensive or extensive. The first are the so-called "roof gardens", consisting of large shrubs or trees. They offer many benefits, such as improving air quality, enhancing the sound and thermal insulation of buildings, and reducing runoff after rainfall events. However, they are complex, require intensive care, have plants with deep roots, and, even with the use of lightweight materials and underlying substance, pose high weight loadings on the rooftops. Thus, they come with the restriction that they should be placed on building structures that can withstand the additional weight. Finally, they are expensive to install and maintain. On the other hand, extensive green roof systems provide a great alternative since they generally require minimal maintenance and have shallower roots. The plant species utilized are restricted to herbs, grasses, mosses, and drought-resistant and low-growing succulents like sedum [57].

For the abovementioned reasons, extensive GRs were considered as a more applicable nature-based solution to mitigate the UHI effect. Two vegetation types with different characteristics were selected and further evaluated for their ability to reduce air temperature in the urban environment of the GAA: grass (herbaceous lawn) and sedum. The latter is considered more suitable for dry and moderate climates because it can withstand harsh weather conditions [58,59]. However, dealing with sedum can be challenging because its complex transpiration mechanism is not well parameterized in standard vegetation models, and providing accurate input values for this type of vegetation is difficult due to the limited data published [60]. The physical characteristics used for grass and sedum were proposed by [61] and are summarized in Table 1.

**Table 1.** Physical parameters of the two roof greening options.

| Green Roof Parameters | Grass | Sedum |
|---|---|---|
| Leaf Area Index (LAI) | 2 | 3 |
| Albedo | 0.3 | 0.15 |
| Emissivity | 0.95 | 0.83 |
| Minimal stomatal resistance | 40 | 150 |

Units: LAI ($m^2$ $m^{-2}$); albedo (non-dimensional); emissivity (non-dimensional); minimal stomatal resistance (s $m^{-1}$).

Finally, to examine the sensitivity of the UHI effect to the percentage of rooftop greening, different scenarios of vegetation coverage were also considered. These scenarios are discussed in a following section.

### *3.2. Data and Model Configuration*

The modeling system employed in this study is the mesoscale Weather Research and Forecasting model (WRF v4.3.3) [62]. WRF can incorporate an Urban Canopy Model (UCM) to represent the urban land–atmosphere interactions instead of only relying on the Noah land-surface model, which treats urban areas as horizontally homogeneous surfaces with specific urban surface properties (USPs), such as albedo, surface emissivity, and soil

moisture availability. Using a UCM is a more precise approach since the sources and sinks of heat, momentum, and turbulent kinetic energy (TKE) are not limited to the surface but are distributed vertically throughout the urban canopy [41]. The urban canopy extends from the ground level up to the rooftops.

The UCM employed to assess the effects of urban areas on dynamics, thermodynamics, and the radiation budget within the urban canopy is the BEP/BEM model. This selected parameterization is recognized as one of the most advanced for investigating the Urban Heat Island (UHI) effect, as the BEP/BEM combines a multi-layer Building Effect Parameterization (BEP) scheme with a Building Energy Model (BEM) [41,42,63]. The BEP quantifies the influence of urban buildings and surfaces—both horizontal (roofs and canyon floors) and vertical (building walls)—on momentum, heat, and TKE [41], while the BEM incorporates the anthropogenic heat component, particularly modeling the effects of air conditioning and heat exchange between a building's interior and the external environment. Additionally, the BEP/BEM includes a land-surface scheme for GRs [45,60]. This 1D model (GREEN-ROOF module) calculates energy and moisture budgets by accounting for atmospheric pressure, incoming net radiation, precipitation or irrigation, evapotranspiration, heat exchange, and heat and moisture diffusion from the soil [45]. The model comprises four distinct compartments: a top layer where vegetation interacts with the atmosphere, a growing medium that houses the plant root systems, a drainage layer responsible for hydrological exchange with the upper compartments, and a bottom layer representing the structural components of the building and any artificial roof layers used for waterproofing or thermal insulation [60].

To fully leverage the capabilities of such an advanced urban canopy model, accurate input data on land use and urban form is crucial. In this study, the default urban land-cover categories from MODIS were replaced with 11 new urban categories based on the LCZ classification (Table 2). To address this limitation, a more detailed map generated by the CLIMPACT project was utilized (Figure 3). Within the CLIMPACT framework, the initial LCZ map for Athens was refined to produce a more detailed version. This map was created using remote sensing data, digital elevation models from the Hellenic Cadastre, and GIS data to derive urban morphological parameters such as building height, vegetation height and density, and canyon aspect ratio. A decision tree was then employed to assign each pixel to a specific LCZ based on a range of potential values for urban parameters within each zone [23]. Each pixel is represented by a designated LCZ, thereby linking distinct urban types to critical surface parameters used in the urban simulations (Figure 3).

**Table 2.** Local Climate Zones categories inside LANDUSE table of WRF [64]. They replace the urban categories of MODIS.

| WRF-Urban Classes | LCZ Classes | LCZ Characterization |
|---|---|---|
| 31 | LCZ1 | Compact high-rise |
| 32 | LCZ2 | Compact mid-rise |
| 33 | LCZ3 | Compact low-rise |
| 34 | LCZ4 | Open high-rise |
| 35 | LCZ5 | Open mid-rise |
| 36 | LCZ6 | Open low-rise |
| 37 | LCZ7 | Lightweight low-rise |
| 38 | LCZ8 | Large low-rise |
| 39 | LCZ9 | Sparsely built |
| 40 | LCZ10 | Heavy industry |
| 41 | LCZE11 | Rock and paved [1] |

[1] Extra categories to take into account large asphalt surfaces [45].

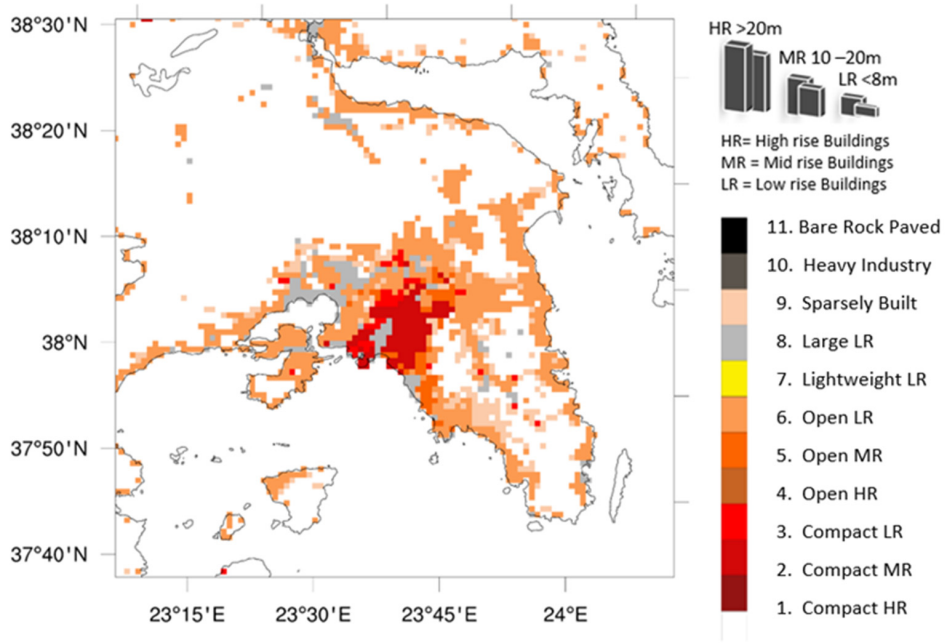


**Figure 3.** Urban categories based on CLIMPACT classification as used in the WRF-Urban simulations with a resolution of 1 km.

### *3.3. Experimental Set-Up*

The WRF-BEP/BEM model was configured to operate with three two-way nested domains. The parent domain covers the entire European continent and Northern Africa with a horizontal resolution of 9 km, which is sufficiently large to capture and generate its own synoptic and mesoscale activities. The first nested grid covers Greece with a resolution of 3 km, while the highest-resolution grid encompasses Attica at a resolution of 1 km (Figure 4). All domains were described vertically by 45 layers. The initial and boundary conditions were obtained from the ERA5 reanalysis dataset (ECMWF), which has a horizontal resolution of 0.25° × 0.25°, and they were updated every 6 h. All analyses were conducted using the hourly outputs from the 1 km grid. Details about the model setup are provided in Table 3.

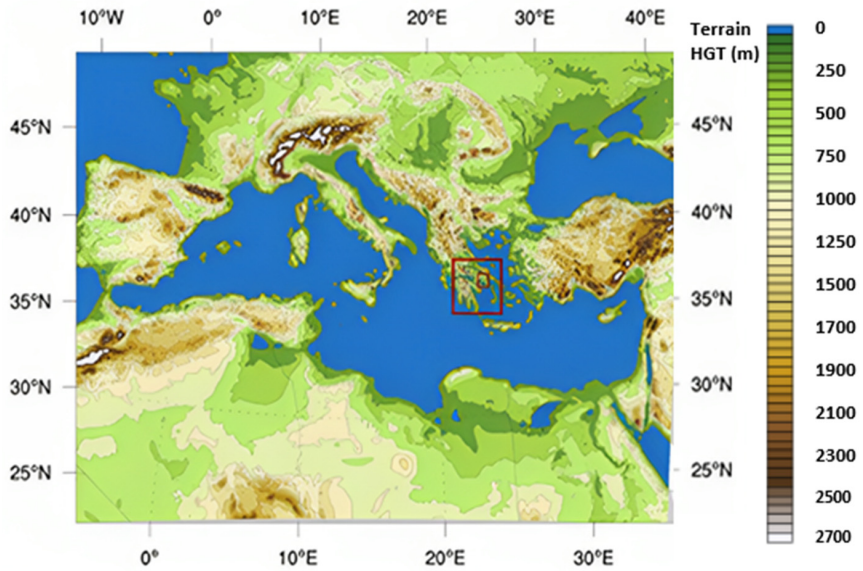


**Figure 4.** The WRF-BEP/BEM domain configuration (terrain height in m). Three two-way nested grids with horizontal resolutions of 9 km, 3 km, and 1 km, respectively. The two nested grids within the outer domain are displayed in the red frames.

**Table 3.** WRF-BEP/BEM set up.

| **Physical Parameterizations** | |
|---|---|
| Land-surface model | Noah–MP (NCEP/Oregon State University/Air Force/Hydrologic Research Lab) [65] |
| Boundary-layer processes | Mellor–Yamada–Janjic TKE scheme [66] |
| Surface-layer processes | Monin–Obukhov (Janjic) scheme [67,68] |
| Urban processes | BEP/BEM parameterization [41,42,65]—The urban scheme used only for the innermost domain |
| Radiation (sw and lw) | RRTM scheme [69] |
| **Input Data** | |
| Land use—Urban areas | CLIMPACT—LCZ [28] for Athens<br>MODIS for the rest of the domain |
| Sea surface temperature | Analysis from Copernicus Marine Environment Monitoring Service (CMEMS)<br>Resolution 0.083° × 0.083° |
| Topography | (a) United States Geological Survey (USGS, 30 arcsec × 30 arcsec),<br>(b) NASA Shuttle Radar Topographic Mission (SRTM, 3 arcsec × 3 arcsec). |

The simulation period was divided into 72 h runs that covered the dates from 28 July to 5 August 2021. The first 12 h of each run were considered as spin-up periods and excluded from the analysis. For each 72 h simulation, a control run (CR) and three greening scenarios were performed and evaluated: scenario 1 (S1): 100% grass coverage; scenario 2 (S2): 100% sedum coverage; scenario 3 (S3): 50% grass coverage (Table 4).

**Table 4.** The greening scenarios adopted in this research.

| **GR Scenarios for the Attica Region** | |
|---|---|
| Control run (CR) | No vegetation |
| Scenario 1 (S1) | 100% total coverage with grass |
| Scenario 2 (S2) | 100% total coverage with sedum |
| Scenario 3 (S3) | 50% total coverage with grass |

For the GR simulations in the GAA, we used similar values to [70] to describe the thermal and physical characteristics of the buildings (and the surrounding roads) according to which LCZ category they have been classified but with specific alternations to better adapt the simulations to the characteristics of Athens. Indicative values for each LCZ category are given in Table 5 below. More information can be found at the official site of WUDAPT.

**Table 5.** Model parameters used for buildings (roofs, walls, etc.) and roads in the GAA. (BH = Building Height; TCR/TCW/TCG = Thermal Conductivity of Roof/Walls/Ground (Road); HCR/HCW/HCG = Heat Capacity of Roof/Walls/Ground (Road); SAR/SAW/SAG = Surface Albedo Roof/Walls/Ground (Road); SER/SEW/SEG = Surface Emissivity Roof/Walls/Ground (Road).)

| **Urban Parameters** | **LCZ2** | **LCZ3** | **LCZ5** | **LCZ6** | **LCZ8** | **LCZ9** |
|---|---|---|---|---|---|---|
| BH Units: (m) | 17.5 | 6.5 | 17.5 | 6.5 | 6.5 | 6.5 |
| TCR/TCW/TCG Units: (MJ $m^{-1}$ $s^{-1}$ $K^{-1}$) | 1.25/1.5/0.73 | 1/1.25/0.69 | 1.25/1.45/0.62 | 1/1.25/0.6 | 1.25/1.25/0.51 | 1/1/0.55 |
| HCR/HCW/HCG Units: (MJ $m^{-3}$ $K^{-1}$) | 1.8/2.67/1.68 | 1.44/2.05/1.63 | 1.8/2/1.5 | 1.44/2.05/1.47 | 1.8/1.8/1.38 | 1.44/2.56/1.37 |
| SAR/SAW/SAG Units: - | 0.18/0.2/0.14 | 0.15/0.2/0.14 | 0.13/0.25/0.14 | 0.13/0.25/0.14 | 0.18/0.25/0.14 | 0.13/0.25/0.14 |
| SER/SEW/SEG Units: - | 0.91/0.9/0.95 | 0.91/0.9/0.95 | 0.91/0.9/0.95 | 0.91/0.9/0.95 | 0.91/0.9/0.95 | 0.91/0.9/0.95 |

The model outputs were evaluated by comparing them with the measurements from five conventional meteorological stations located in Harokopio University of Athens (Kallithea-HUA) near the city's center, in Agia Paraskevi (northeast), Tatoi (north), Eleysina (northwest), and Elliniko (south). Their exact locations are given in the map of Figure 5.

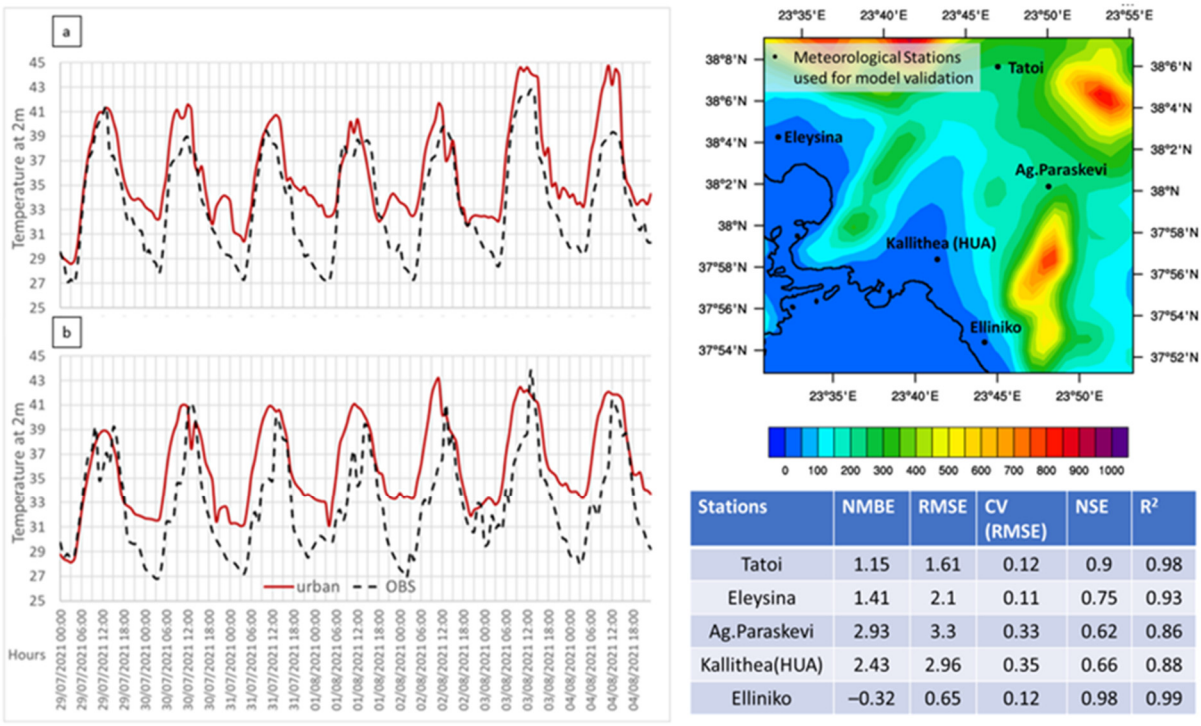


| Stations | NMBE | RMSE | CV (RMSE) | NSE | $R^2$ |
|---|---|---|---|---|---|
| Tatoi | 1.15 | 1.61 | 0.12 | 0.9 | 0.98 |
| Eleysina | 1.41 | 2.1 | 0.11 | 0.75 | 0.93 |
| Ag.Paraskevi | 2.93 | 3.3 | 0.33 | 0.62 | 0.86 |
| Kallithea(HUA) | 2.43 | 2.96 | 0.35 | 0.66 | 0.88 |
| Elliniko | −0.32 | 0.65 | 0.12 | 0.98 | 0.99 |

**Figure 5.** Comparison of temperature at 2 m (°C) between model control run and observations from two meteorological stations in Attica: (**a**) HUA and (**b**) Agia Paraskevi. On the right part of the figure, the topographic map (height scale in m) with the locations of the selected stations is given along with the table with the statistical measurements (between model and observation) for each station.

The comparison shows that the model accurately depicted the daily evolution of temperature at 2 m at all stations. However, as can be detected from the table with the statistics, it overestimated the temperature at 2 m in all stations except from Elliniko. This overestimation in the region of HUA, especially at night, can be explained: Although the meteorological station at HUA is located very close to the center of Athens (dense construction, with buildings of 3–9 floors and absence of green spaces; LCZ2), the microclimate of the specific station's location differs enough because it is inside the university campus surrounded by relatively high trees. Between the HUA station and Agia Paraskevi station, the overestimation is less pronounced in Agia Paraskevi for 3 August 2021 but greater during the period from 1 August 2021 to 2 August 2021 for both day and night. The calculated statistical measurements are the Normalized Mean Bias Error (NMBE), the Root Mean Square Error (RMSE), the Coefficient of Variation of RMSE (CV(RMSE)), the Nash–Sutcliffe model Efficiency coefficient (NSE), and the correlation coefficient ($R^2$). Higher positive values of NSE closer to 1 indicate better model performance. Specifically, the model performance is good for NSE values greater than 0.35 and exceptional for values greater than 0.9. By comparing the NSE values among the stations, the model shows a generally high performance, with the Elliniko and Agia Paraskevi stations showing the maximum and minimum validation values, respectively.

## 4. Results

As discussed before, implementing GRs can significantly mitigate urban heating and reduce urban temperatures. To demonstrate the magnitude of this improvement under varying local conditions during Athens' extreme HW event in 2021, two dates with different characteristics were chosen and further analyzed: 2 August 2021 and 3 August 2021. These two dates differ in their prevailing winds. In the first case, the SB dominated over the weak northerly flow and managed to reach the northern sector of the GAA, whereas in the second case, the prevailing northern flow and the resulting heat island acted as barriers,

preventing the SB from penetrating inland and limiting its effects only on the coastal areas (Figures 6 and 7). In both cases, there was an interaction between the synoptic (Etesians) and the local thermal circulations, which determined where the maximum temperatures occurred, depending on which flux was more powerful.

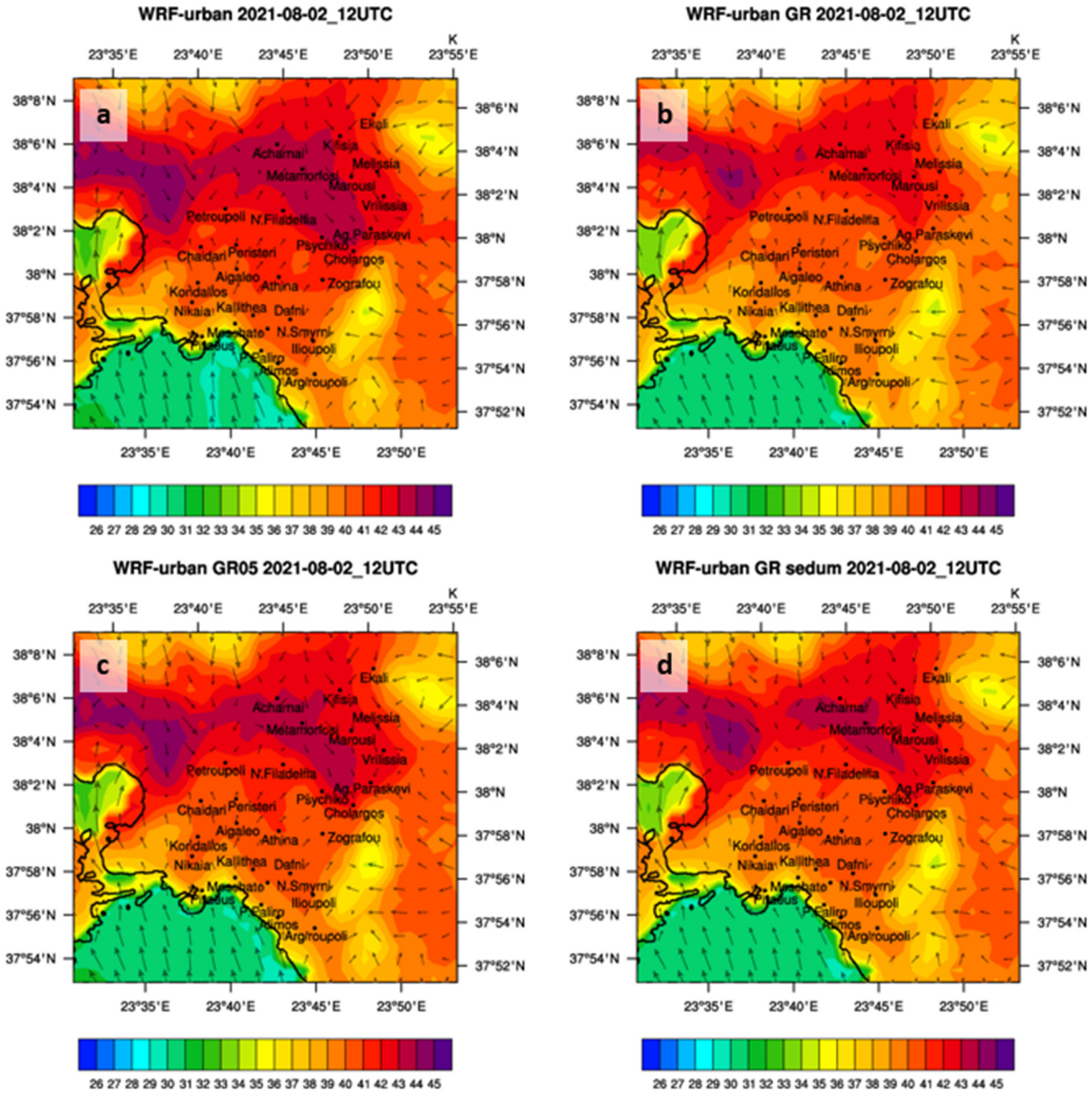


**Figure 6.** Temperature at 2 m (°C) over the GAA for 2 August 2021 at 12:00 UTC (dominant circulation—SB). The control run and the three greening scenarios for the rooftop are presented: (**a**) control run—roofs without vegetation; (**b**) roofs covered 100% by grass; (**c**) roofs covered 50% by grass; (**d**) roofs covered 100% by sedum.

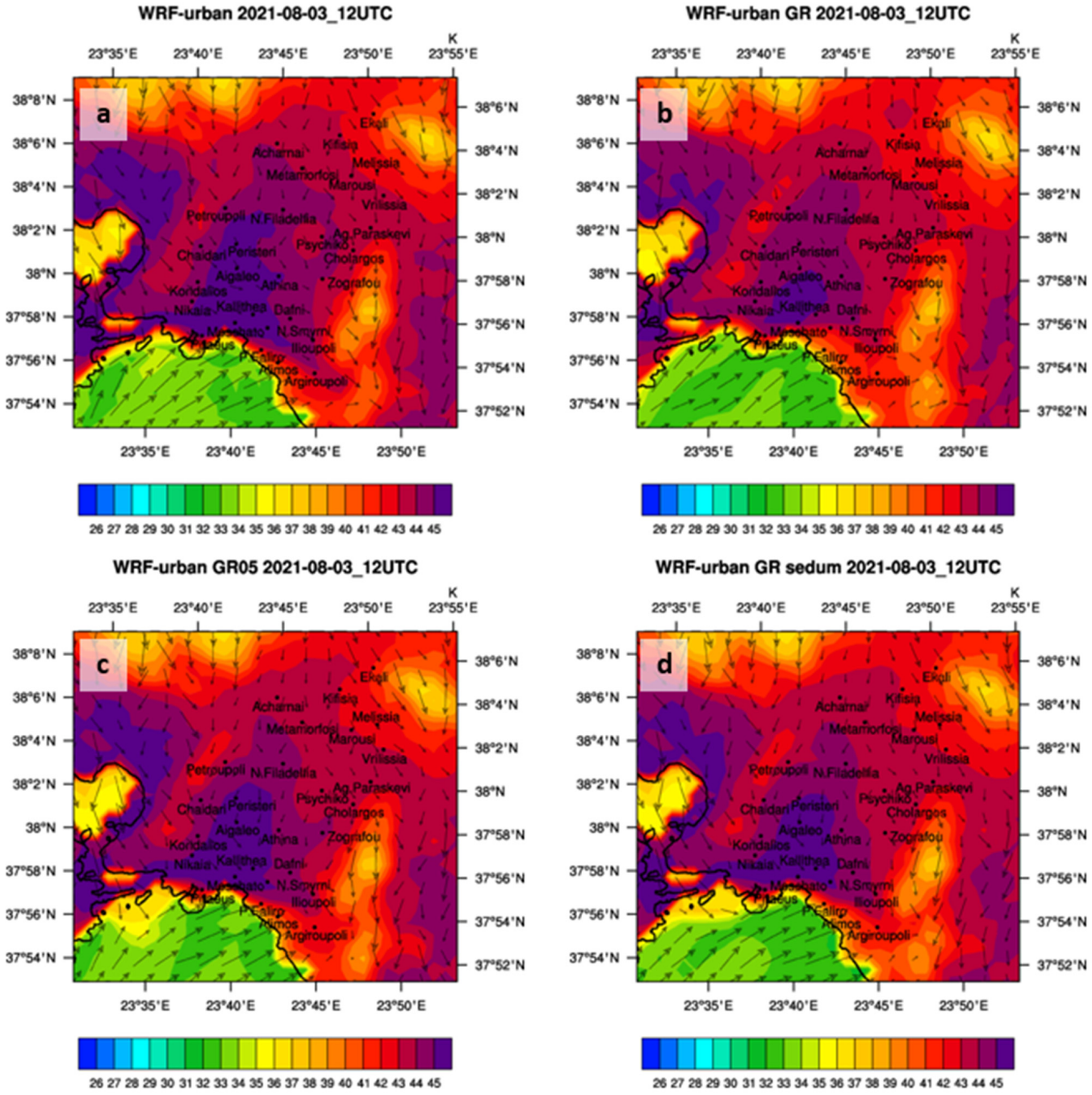


**Figure 7.** Temperature at 2 m (°C) over the GAA for 3 August 2021 at 12:00 UTC. The control run and the three greening scenarios for the rooftop are presented: (**a**) control run—roofs without vegetation; (**b**) roofs covered 100% by grass; (**c**) roofs covered 50% by grass; (**d**) roofs covered 100% by sedum.

Regarding the 2nd of August 2021, the GAA was influenced by a weak northeast flow (1–2 m/s), which allowed the SB to evolve and extend to the northern suburbs (Figure 6). As a result, the highest temperatures were evident in the northern suburbs (Nea Filadelfia, Petroupoli, Metamorfosi, Marousi, Acharnai, Kifisia, etc.), where the influence of the SB was diminished (Figure 6). The central and coastal areas experienced temperatures 1–3 °C lower than those in the northern areas (Figure 6).

Implementing the GR scenarios resulted in a reduction in the temperature field of about 0.5–2 °C over the entire GAA, except for the coastal areas, which remained almost unaffected (Figure 6). The greatest temperature reductions are evident in the north and north-eastern suburbs (Figure 7). In most of the studied suburbs, the reduction exceeded

0.5 °C during the peak daytime hours. Comparing three areas—one in the southern suburbs, one in the center of the GAA, and one in the northern sector—it is evident that the daily variability of temperature at 2 m was strongly controlled by the SB evolution, especially for Moschato (southern suburb) and Athens (city center). In all cases, the implementation of GRs reduced daytime temperature. The most important reduction occurred in Athens's city center, starting from 07 UTC and lasting until 16 UTC. In Kifisia, despite experiencing the highest temperatures, the impact of GRs was smaller, with peak effects occurring between 14 UTC and 17 UTC (Figure 8).

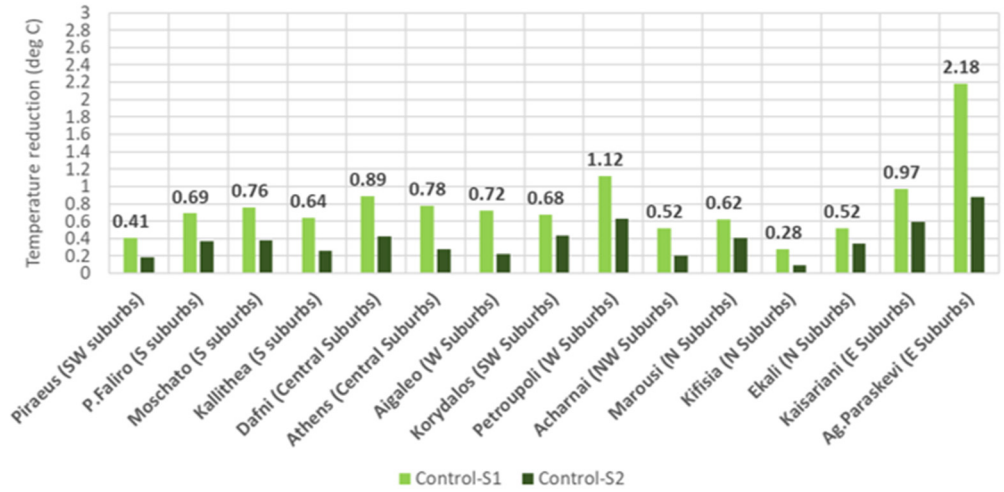


**Figure 8.** Histogram representing the decrease in 2 m temperature (°C) due to the implementation of GRs, namely CR (no vegetation)—S1 (grass 100%) and CR (no vegetation)—S2 (sedum 100%), across various indicative regions around Athens for 2 August 2021, 11–13 UTC (SB day).

When comparing the scenarios with the control simulation, it is evident that scenario S1 (100% grass) provided the most significant benefits, followed by scenario S2 (100% sedum) (Figure 6a,b). Grass outperformed sedum at all selected locations. Grass seems to efficiently alter the heat balance by converting solar radiation into latent heat flux through evapotranspiration and thus increasing the cooling effect of the surrounding environment (Figures 8 and 9). Additionally, the higher albedo of grass contributes to daytime cooling by reflecting more solar radiation and absorbing less heat.

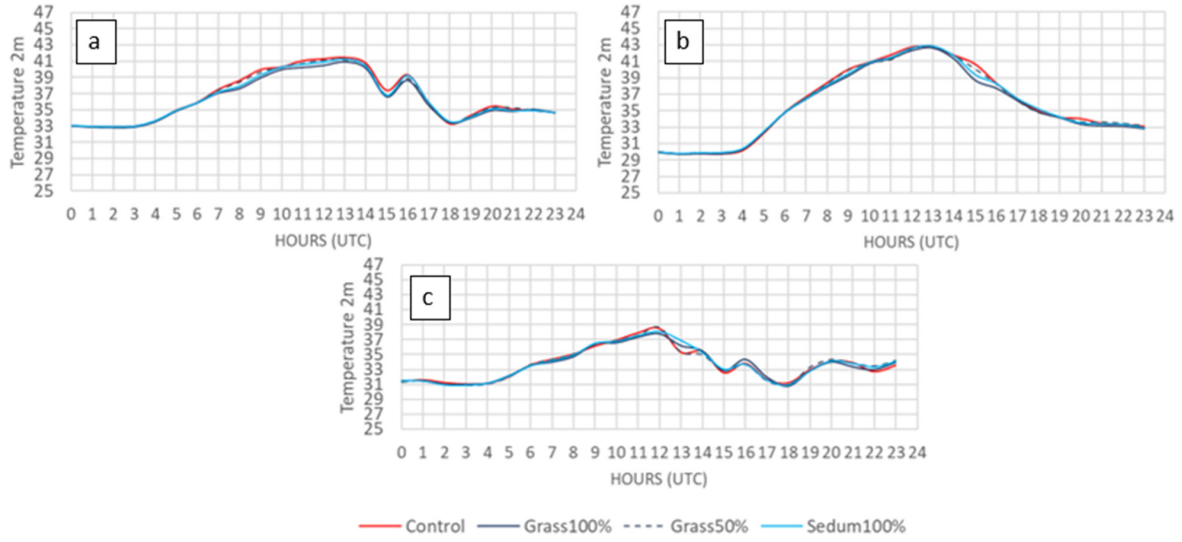


**Figure 9.** Daily variability of temperature at 2 m (°C), control run (red line), grass 100% (dark-blue line) sedum 100% (light-blue line), and grass 50% (dashed line). (**a**) Athens (central suburbs), (**b**) Kifisia (northern suburbs), and (**c**) Moschato (southern suburbs) for 2 August 2021.

During nighttime, the effect of GRs on the ambient temperature was much smaller compared to daylight hours (Figure 10). This is because the main cooling mechanism of vegetation, i.e., evapotranspiration, in the absence of sunlight is negligible. Comparing the two vegetation types, during the night, grass provided better results due to its higher emissivity compared to sedum, which allowed grass to release more longwave radiation into the surrounding space, keeping the surface cooler (Figure 10).

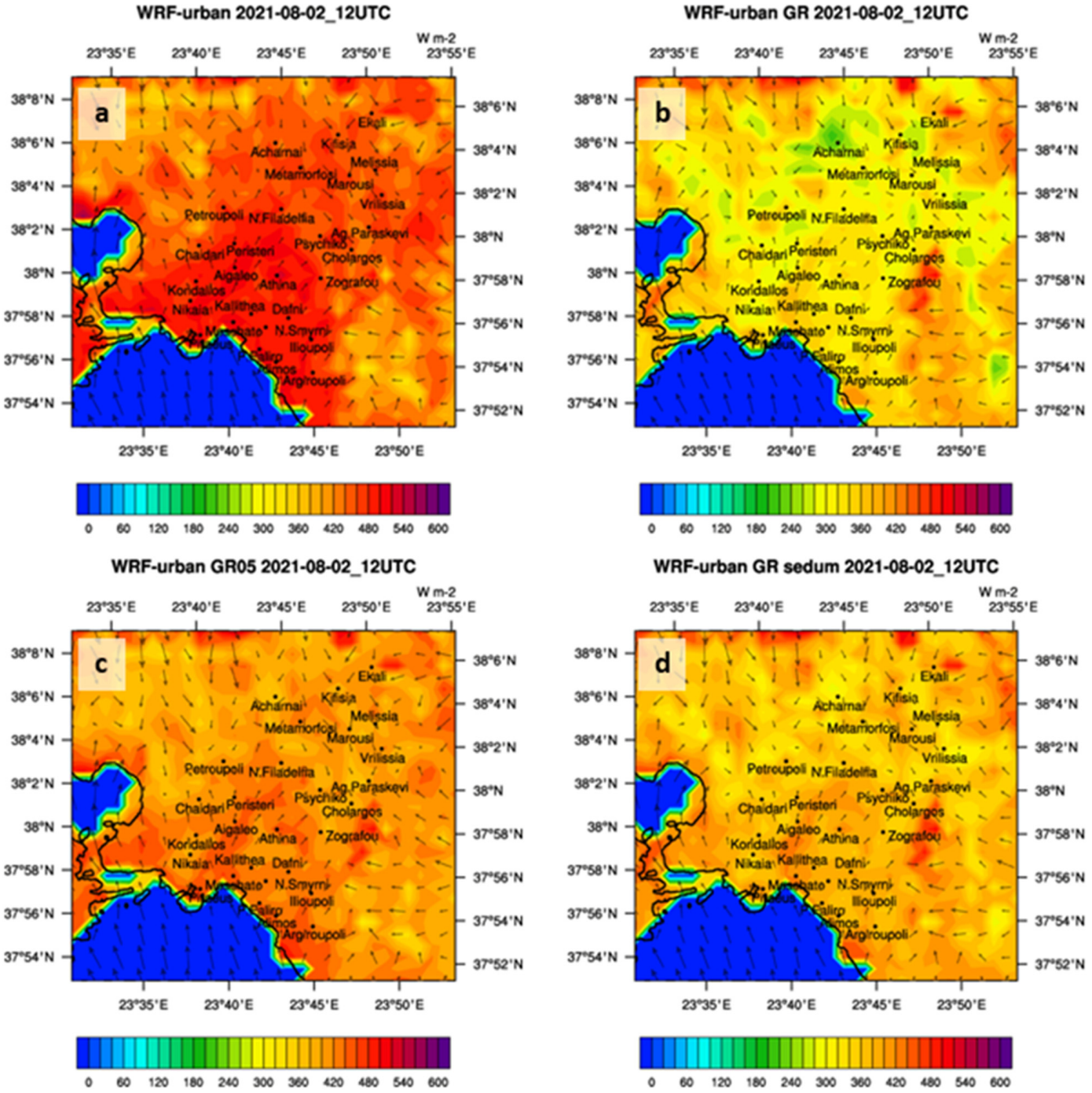


**Figure 10.** Sensible heat flux (W $m^{-2}$) for the day of the HW with SB, 02/08/2021 12 UTC, for the control run and the three different green roof scenarios. (**a**) Control run (no rooftop cover), (**b**) grass 100%, (**c**) grass 50%, and (**d**) sedum 100%.

When testing the impact of varying coverage percentages on urban heat mitigation, it was found that reducing rooftop green coverage to 50% (Scenario S3—50% grass) resulted in minimal temperature reduction that can be considered negligible (Figure 6c).

On 3 August 2021, the dominant circulation was the Etesians, with wind speeds ranging from 2 to 3 m/s and coming from the northeast (Figure 7). This was the hottest day of the HW. The center of the heat island, where the highest temperatures were simulated, was located in the southern and central part of the GAA, extending from Piraeus and Moschato north towards Nea Filadelfia (Figure 7). The sensible heat flux during this day was higher compared to the previous one (Figures 10 and 11). High temperatures were also observed in the center of Athens and the surrounding suburbs, with intensity varying throughout the day and peaking at 12 UTC. The extremely high temperatures in these areas developed an intense local thermal circulation that, along with the northerly flow, acted as a barrier, deflecting the SB towards Palaio Faliro and Alimos (Figures 7 and 12).

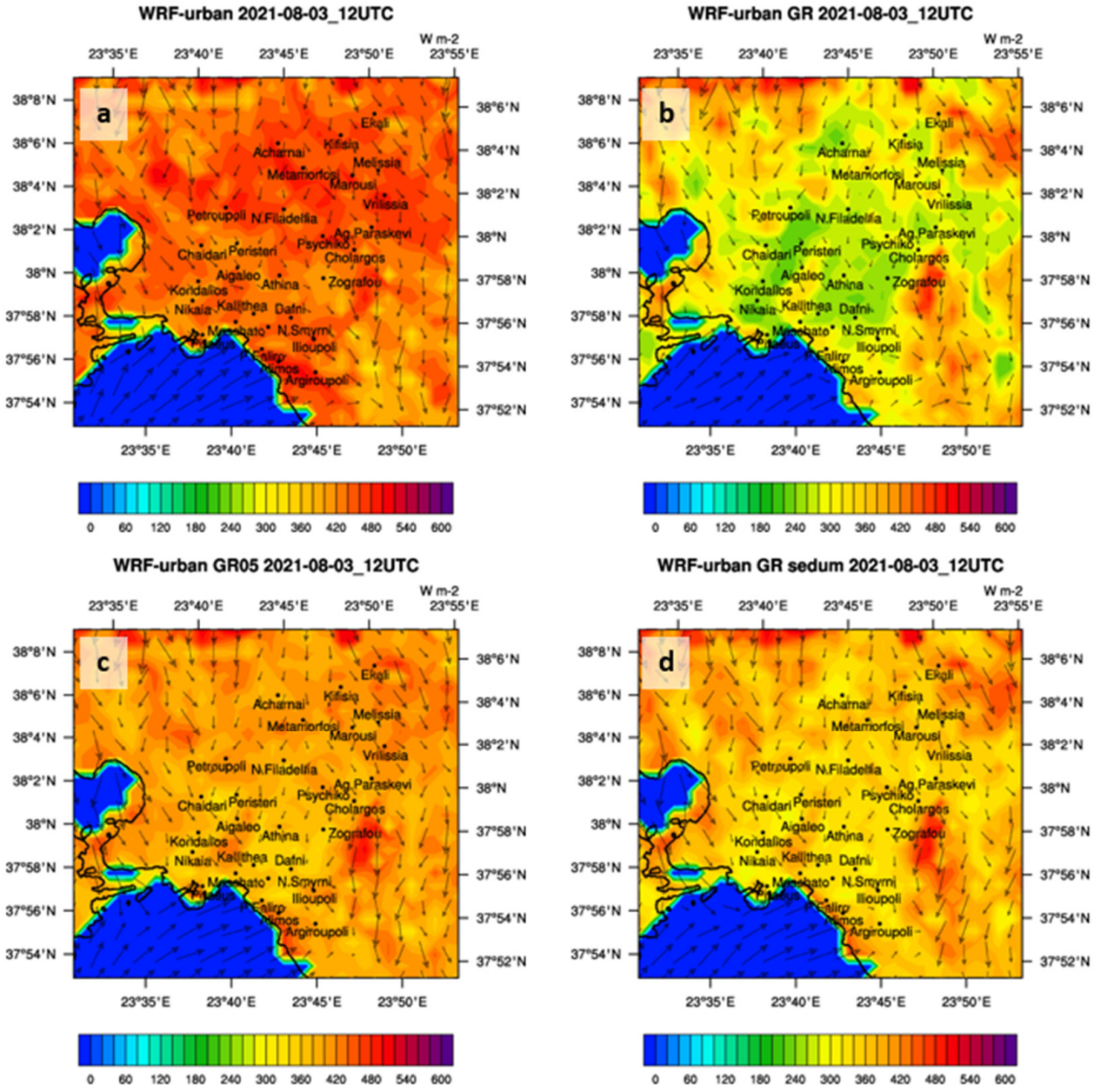


**Figure 11.** Sensible heat flux (W $m^{-2}$) for the hottest day of the HW, 3 August 2021 12 UTC, for the control run and the three different green roof scenarios. (**a**) Control run (no rooftop cover), (**b**) grass 100%, (**c**) grass 50% and (**d**) sedum 100%.

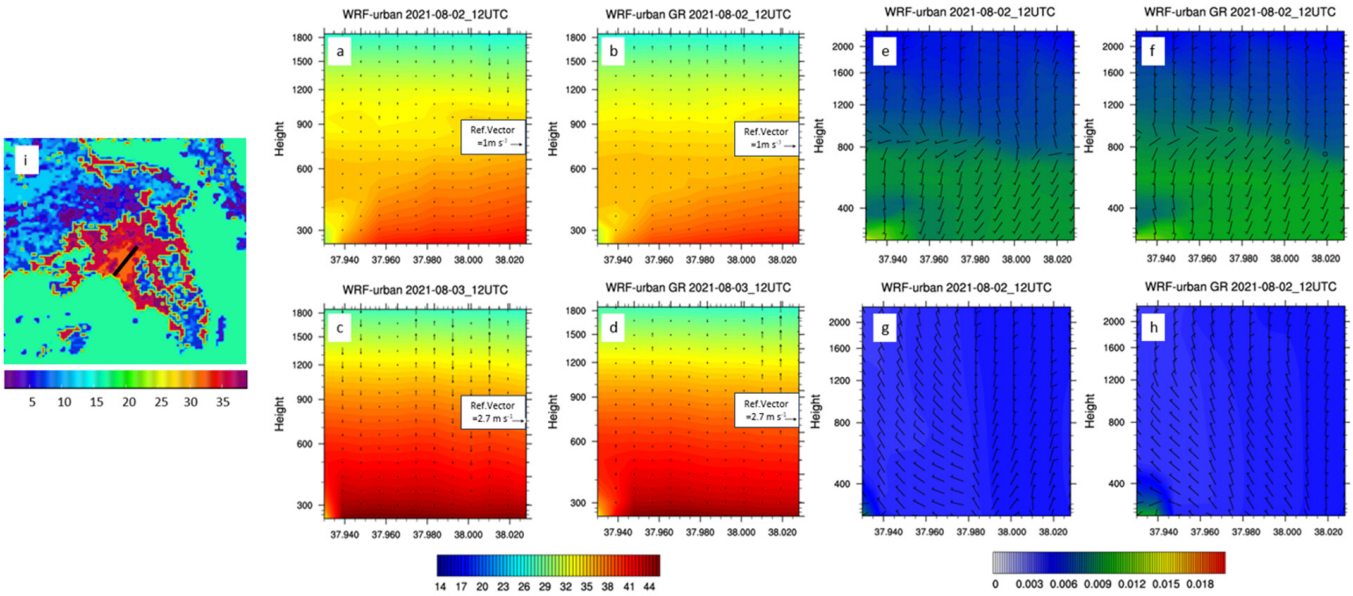


**Figure 12.** Left panel (**a**–**d**): Vertical cross-section of temperature (°C) and vertical wind speed (m $s^{-1}$) for 2 August 2021 ((**a**) control run: no rooftop cover and (**b**) scenario: 100% grass) and 3 August 2021 12 UTC ((**c**) control run: no rooftop cover and (**d**) scenario: 100% grass). Right panel (**e**–**h**): Vertical cross-section of relative humidity (kg $kg^{-1}$) and wind speed (m $s^{-1}$) (wind barbs) for 2 August 2021 ((**e**) control run: no rooftop cover and (**f**) scenario S1: 100% grass) and 3 August 2021 12 UTC ((**g**) control run: no rooftop cover and (**h**) scenario S1: 100% grass), (**i**) the black line in the map of Attica is the cross-section on which the other figures are referred. The cross-section line is shown in black on the map on the left (colored bars on the map show the distribution of land-use values in Attica).

The implementation of GRs led to a temperature reduction of 0.5–1 °C in most areas of the basin, along with a reduction in sensible heat flux that was higher than the previous day (Figures 7, 10 and 11). Notably, GRs reduced the intensity of the thermal center and the vertical movements over the central and southern suburbs, which allowed the SB to penetrate further into the southern areas (Figures 7 and 12). This contributed to a further cooling effect of about 2 °C in the southern suburbs (Figures 7 and 13). Changes in wind circulation can be attributed to alterations in the local heat balance of the lower atmosphere, caused by modification of the thermodynamical properties of the urban area through the implementation of GRs. Covering buildings with GRs reduced the maximum temperatures and altered their spatial distribution. Specifically, the center of the UHI shrank, covering a smaller area situated in the southern part of the GAA surrounded by Moschato, Kallithea, and Aigaleo. Moving northward towards the city center, the temperature reductions ranged between 0.6 °C and 0.7 °C in the western, eastern, and central suburbs. In the northern suburbs, the reduction in temperature was smaller, with values not exceeding 0.4 °C (Figure 13).

The daily variability of temperature was influenced by the SB only at the southern location of Moschato, while the other two locations, Athens and Kifisia, followed the solar radiation cycle (Figure 14). In the city center, which experienced the highest temperatures during the day, the reduction due to GRs was particularly noticeable between 07:00 and 17:00 UTC compared to the other locations, experiencing two peaks: one at 08 UTC (0.8 °C) and the other at 13 UTC (1 °C) (Figure 14).

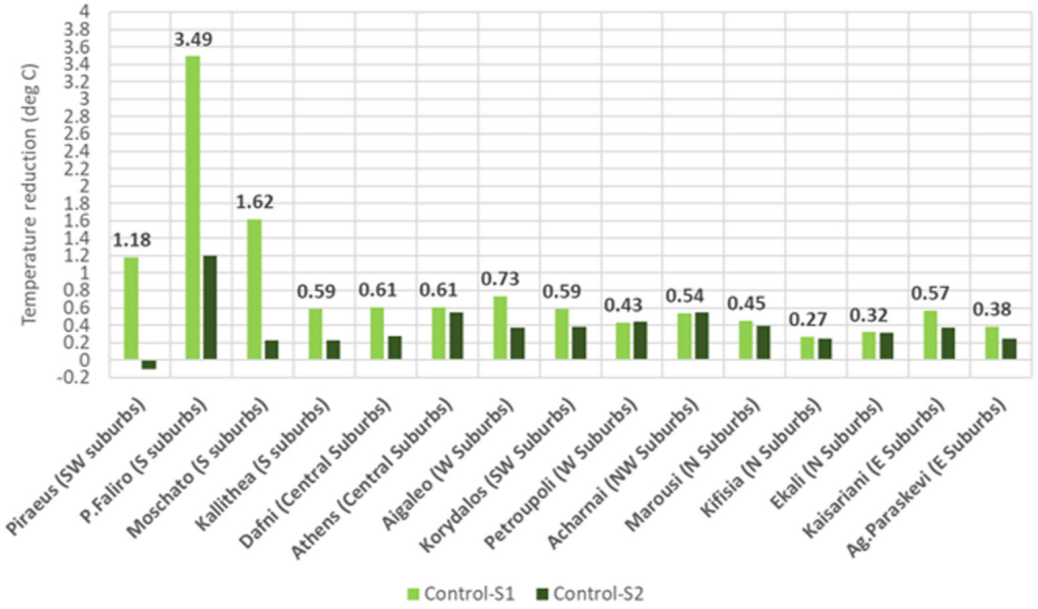


**Figure 13.** Histogram representing the decrease in 2 m temperature (°C) due to the implementation of GRs, namely CR (no rooftop cover)—S1 (grass 100%) and CR (no rooftop cover)—S2 (sedum 100%), across various indicative regions around Athens for 3 August 2021, 11–13 UTC.

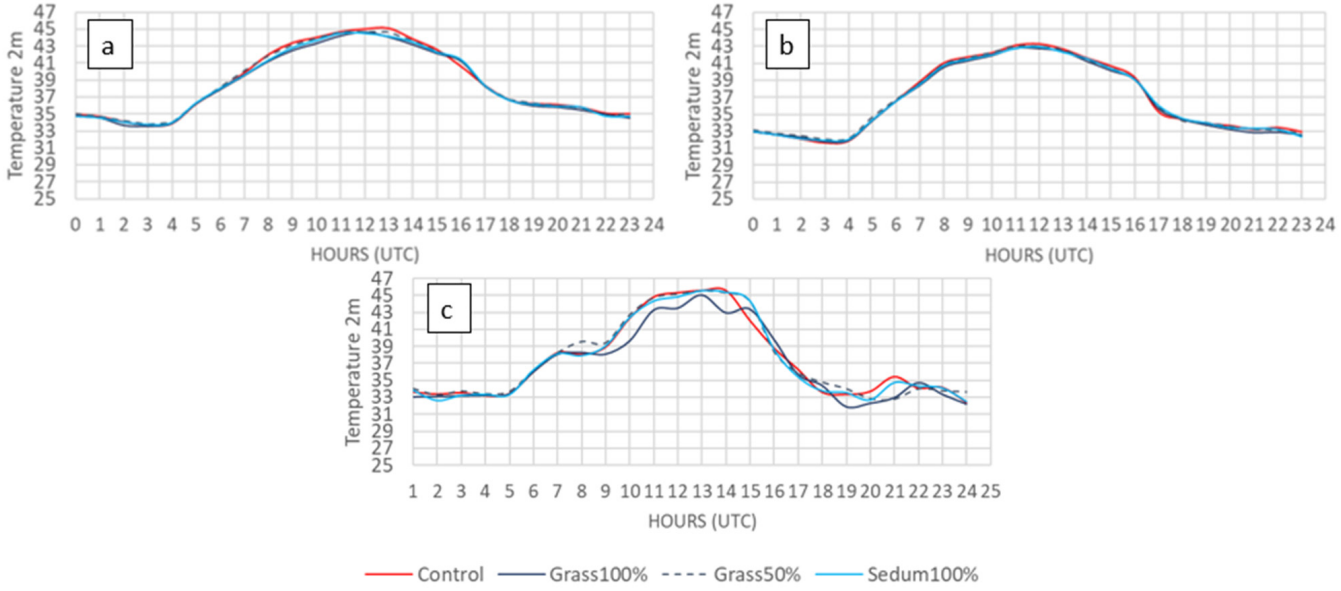


**Figure 14.** Daily variability of temperature at 2 m (°C), control run (red line), grass 100% (dark-blue line), sedum 100% (light-blue line), and grass 50% (dashed line). (**a**) Athens (central suburbs), (**b**) Kifisia (northern suburbs), and (**c**) Moschato (southern suburbs) for 3 August 2021.

During this day, full coverage with either sedum or grass yielded similar results, while during the SB day, grass outperformed sedum (Figures 6, 7, 10 and 12). Reducing the rooftop green coverage to 50% (Scenario S3—50% grass) resulted in a very small temperature reduction of less than 0.2 °C, which can be considered negligible (Figure 7d).

In summary, the temperature field revealed a spatial and temporal variability during the day (Figures 14 and 15). This variability was controlled by the interaction of SB, UHI circulation, and the Etesians. These circulations, ranging from local to synoptic scales, are thermally driven and peak around noon. GRs modified the thermal distribution across the GAA, affecting the timing and intensity of these local thermal circulations (Figures 6 and 7). When the northerly winds, i.e., Etesians, are stronger than the SB, the highest temperatures

are typically found in the southern parts of the GAA. This happens because, as the air travels over the heated urban landscape, it accumulates more heat the farther it travels [71]. Conversely, when the dominant wind direction is from the south, driven by SB, the highest temperatures are met in the northern regions of the GAA.

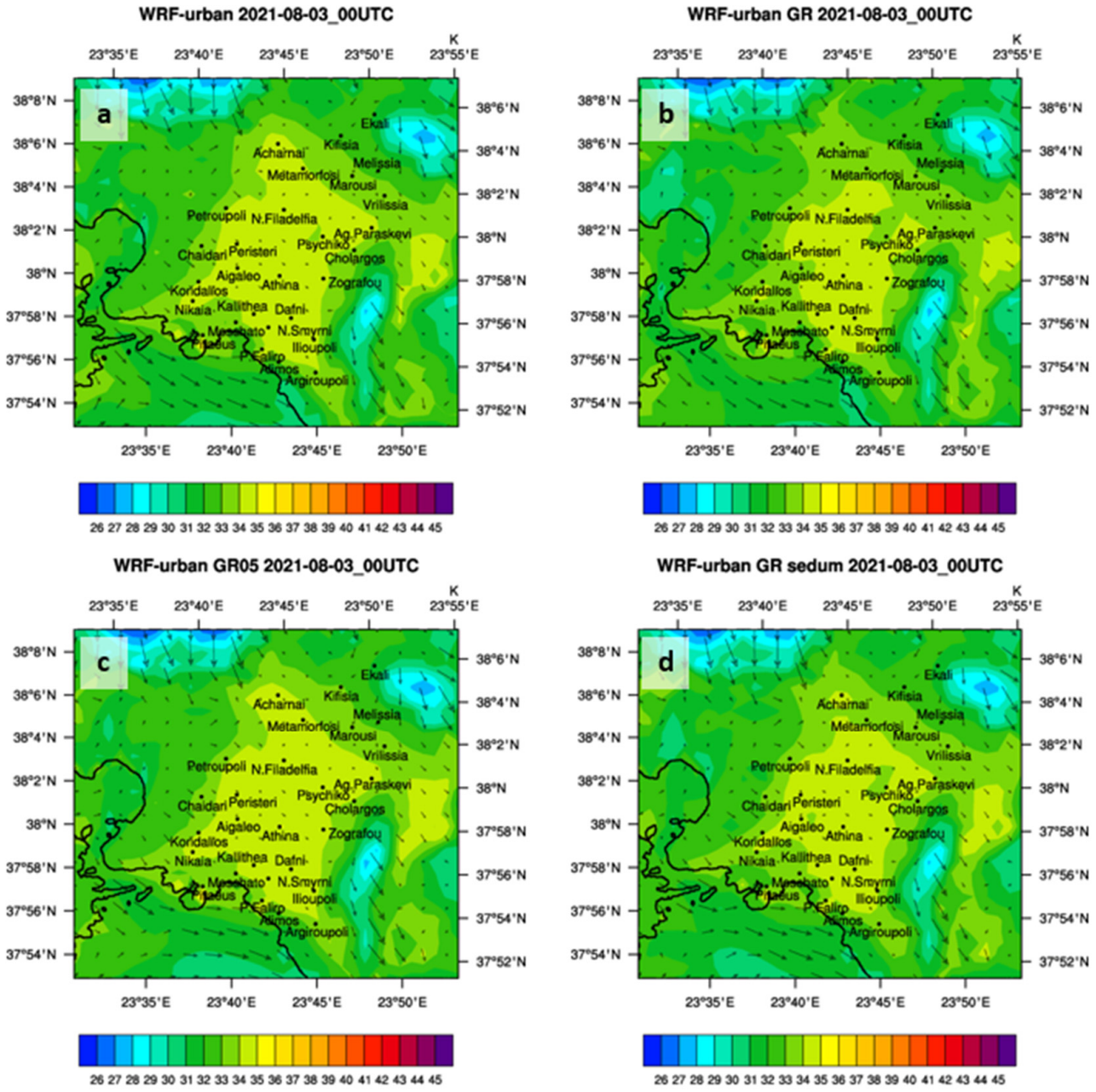


**Figure 15.** Temperature at 2 m (°C) for the hottest day of the HW, 3 August 2021 00:00 UTC, for the control run and the three different green roof scenarios. (**a**) Control run (no rooftop cover), (**b**) grass 100%, (**c**) grass 50%, and (**d**) sedum 100%.

The effectiveness of GRs differs from area to area based on the local climate (wind conditions and temperatures) and geographic location (proximity to the sea). It is evident that in coastal areas such as the GAA, GRs have a dual role in mitigating urban heating. They can either have a direct effect by increasing the latent heat flux through evapotranspiration and thus reducing the ambient temperature or an indirect effect by altering the local thermal circulations such as SB or other localized wind patterns that, in a second phase,

affect the movement of air and heat across the urban area, thus controlling the cooling rate of the air.

On 2 August 2021 (SB day), the dominant effect was the indirect effect. The existence of GRs modified the intensity of the SB by reducing the temperature over land and increasing the temperature gradient between sea and land, resulting in a more intense SB circulation (Figure 6). This alteration seems to be the main cause of the temperature reduction during this day. When comparing the two vegetation types, grass, as discussed before, is more capable of reducing the ambient temperature compared to sedum, and thus, it can intensify the SB circulation, revealing a profoundly better cooling capability (Figure 6).

On 3 August 2021, which is a day where the SB was absent, the direct effect of GRs was the key regulator of the temperature reduction, especially in the central and northern regions. In the coastal areas, the improvement was controlled again by the indirect effect since they are influenced by the SB (Figures 12 and 13). Comparing the two effects of GRs, the indirect effect is stronger; thus, the day with the greatest reduction in temperatures was the first one (strong SB), while comparable results are also evident during the second day in the coastal regions (Figures 10 and 13). Finally, it is worth mentioning that grass and sedum revealed similar effectiveness under conditions where the direct effect was more pronounced (absence of SB), while the opposite is the case when the indirect effect of GRs was the dominant mechanism (SB day; Figures 8 and 13).

At night, when the wind field tended to be weaker, and the temperature differences between sea and land were less pronounced, the highest temperatures were generally found around the center of Athens (Figure 15).

Apart from the benefits discussed, GRs can also have an adverse effect on urban areas since they can reduce the sensible heat flux, which leads to lower vertical wind speeds and reduced vertical mixing. This, in turn, can decrease the height of the planetary boundary layer, resulting in a longer retention time for polluted air near the surface, causing possible air quality issues (Figure 12).

The total efficiency of GR implementations in the city of Athens throughout the day can be seen in Figure 16, which contains the timeseries of the mean 2 m temperature reductions with S1 in the central area of Athens, Kifisia, and Moschato from the days 2 August 2021 and 3 August 2021, which were the hottest days of the studied heatwave.

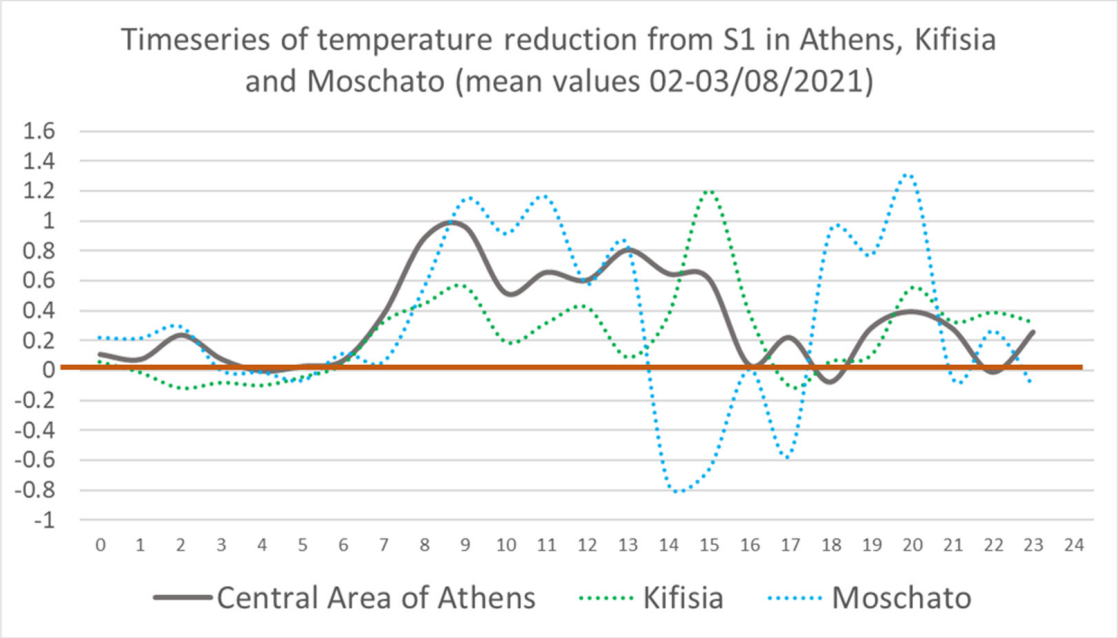


**Figure 16.** Timeseries of the mean 2 m temperature reductions (°C) (00:00 UTC–23:00 UTC) achieved with S1 (grass 100%). The mean values were calculated from 2 August 2021 and 3 August 2021, which were the hottest days during the HW that occurred in 2021.

For the central area of Athens, there was a reduction between 0.5 °C and 1 °C in the hours from 6:00 to 16:00 UTC (or 9:00 to 19:00 local time), while at nighttime, the reduction magnitude reached 0.4 °C at 20:00 UTC (or 23:00 local time). For Kifisia, there was a total reduction throughout the day, which was amplified at 15:00 UTC (or 18:00 local time), exceeding 1 °C. The reductions were also increased at nighttime between 20:00 and 23:00 UTC in this region. In Moschato, the reductions show two maxima, with the first between 07:00 UTC and 13:00 UTC, with the pick value exceeding 1 °C, and between 18:00 UTC and 21:00 UTC, the second maxima had a pick of 1.3 °C. It is noteworthy that in the interim period between those maxima, the reductions are negative, which means that the simulation with S1 between 14:00 UTC and 17:00 UTC (or 17:00 to 20:00 local time) resulted in increased temperatures. Generally, in the Moschato region, the temperature reductions on 2 August 2021 and 3 August 2021 showed a very different behavior, and both days had significant variations. Overall, GR implementation showed a significant reduction during the daytime, which was constant and relatively increased in the central region of Athens, where the heat stress during a HW is more intense.

## 5. Conclusions

HWs and prolonged hot and dry periods make the city of Athens one of the most vulnerable cities to the observed climate overheating trend because it is densely built and significantly lacks green spaces. One relatively costless and beneficial way to absorb the accumulated heat stress in the city of Athens is GRs as a nature-based solution, and the evaluation of their performance regarding temperature reduction using the most recent simulation techniques is of vital importance. In the GAA, a coastal region surrounded by mountains, assessing the effectiveness of GRs in reducing urban heating is challenging. Geographic factors such as proximity to the sea, complex topography, regional climatology, and mesoscale atmospheric flows significantly impact the success of nature-based solutions like GRs. The area is affected by various interacting circulations, including synoptic flow (Etesians), SBs, and UHI circulation. These interactions become particularly important during HWs: The heat island circulation strengthens, synoptic flow weakens, and the SB may either enhance the heat island effect by shifting its center northward or be suppressed by the intense thermal core, leaving the heat island located over the southern and central suburbs.

To assess the impact of GRs on mitigating urban heating in such a complex environment, the atmospheric modeling system WRF was utilized, incorporating specific urban schemes (the multi-layer urban canopy BEP/BEM parameterization) and the most updated land-use categorization (LCZ—CLIMPACT) product for Athens. This study focused on an extreme HW event during the summer of 2021. Three GRs scenarios were compared against a control run without GRs: (a) 100% grass, (b) 50% grass, and (c) 100% sedum.

The implementation of GRs had varying impacts across different parts of the city. GRs affect the atmospheric temperature either directly by changing the latent and sensible heat fluxes or indirectly by altering the local circulations' urban heat island effect and SB. GRs have a stronger indirect effect, and thus, the highest benefits are evident where SB circulation is present.

Overall, covering rooftops entirely with grass can reduce temperatures by approximately 0.7 °C in the central areas of the GAA, including the city center, with reductions reaching 1 °C and higher depending on the area and prevailing wind conditions.

Grass is the most effective vegetation for mitigating urban heating because it is more efficient at converting solar radiation into latent heat flux and has a higher albedo compared to sedum. This difference is more pronounced when SB circulation is involved (indirect effect of GRs); in other cases, the performance of grass and sedum seems to be similar (direct effect of GRs). It is worth mentioning that sedum is more suitable for dry and moderate climates due to its resilience under such conditions.

GRs are more effective during the daytime. This is because greening reduces ambient temperature mainly through evapotranspiration, which only occurs during daylight.

The extent of the coverage is another critical factor; reducing the coverage to half significantly reduces the cooling effect.

GRs modify the daytime boundary layer, including the vertical wind and temperature profiles, by altering the surface energy balance through changes in sensible and latent heat flux. This can sometimes lead to adverse effects on air pollution.

**Author Contributions:** The individual contributions of the authors are: Conceptualization, C.S., M.L., C.Z. and P.K.; methodology, C.S., P.K., M.L. and M.K.; software, P.-M.S., C.M. and A.P.; validation, C.S., P.K. and M.K.; formal analysis, C.S., M.K. and P.-M.S.; investigation, C.S., P.K., P.-M.S. and C.M.; resources, P.K.; data curation, P.-M.S. and C.M.; writing—original draft preparation, P.-M.S., A.P. and C.M.; writing—review and editing, C.S., P.K. and M.K.; visualization, P.-M.S.; supervision, P.K. and M.L.; project administration, M.L.; funding acquisition, M.L. All authors have read and agreed to the published version of the manuscript.

**Funding:** This research has been co-financed by the European Regional Development Fund of the European Union and Greek national funds through the Regional Operational Program "ATTIKI"–ESPA 2014–2020, in the context of NESTOR project ATTP4-0317076.

**Institutional Review Board Statement:** Not applicable.

**Informed Consent Statement:** Not applicable.

**Data Availability Statement:** The data presented in this study are available on request from the corresponding author.

**Acknowledgments:** This work was partly supported by computational time granted from the Greek Research & Technology Network (GRNET) in the National HPC facility-ARIS. The European Centre for Medium-Range Weather Forecasts (ECMWF) is also acknowledged for the provision of the ERA5 dataset and the records from the meteorological stations at Eleysina, Tatoi and Elliniko operated by the Hellenic National Meteorological Service. Harokopio University of Athens provided the measurements from Kallithea and Agia Paraskevi stations.

**Conflicts of Interest:** Authors Michael Loupis and Charis Masouras were employed by the company Innovative Technologies Centre S.A. (ITC). The remaining authors declare that the research was conducted in the absence of any commercial or financial relationships that could be construed as a potential conflict of interest.

## Abbreviations/Nomenclature

| | |
|---|---|
| BEM | Building Energy Model |
| BEP | Building Effect Parameterization |
| BH | Building Height |
| CLIMPACT | A national network for climate change |
| CR | Control Run |
| CV(RMSE) | Coefficient of Variation of the Root Mean Squared |
| ECMWF | European Centre for Medium-Range Weather Forecasts |
| EnergyPlus | Building energy simulation program |
| ERA5 | ECMWF Reanalysis v5 |
| GAA | Greater Area of Athens |
| GIS | Geographic Information System |
| GR | Green Roofs |
| HCG | Heat Capacity of the Ground (road) |
| HCR | Heat Capacity of the building's Roof |
| HCW | Heat Capacity of the building's Walls |
| HUA | Harokopio University of Athens |
| HW | Heat Wave |
| LCZ | Local Climate Zones |
| MODIS | Moderate Resolution Imaging Spectroradiometer |
| NCEP | National Centers for Environmental Prediction |
| NMBE | Normalized Mean Bias Error |
| NSE | Nash–Sutcliffe model Efficiency coefficient |

| | |
|---|---|
| RMSE | Root Mean Square Error |
| RRTM | Rapid Radiative Transfer Model |
| S1 | Scenario 1—grass 100% coverage |
| S2 | Scenario 2—sedum 100% coverage |
| S3 | Scenario 3—grass 50% coverage |
| SAG | Surface Albedo of the Ground (road) |
| SAR | Surface Albedo of the building's Roof |
| SAW | Surface Albedo of the building's Walls |
| SB | Sea Breeze |
| SEG | Surface Emissivity of the Ground (road) |
| SER | Surface Emissivity of the building's Roof |
| SEW | Surface Emissivity of the building's Walls |
| SRTM | NASA Shuttle Radar Topographic Mission |
| TCG | Thermal Conductivity of ground (road) |
| TCR | Thermal Conductivity of the building's roof |
| TCW | Thermal Conductivity of the building's Walls |
| TKE | Turbulent Kinetic Energy |
| TRNYS | Transient System Simulation Tool |
| UCM | Urban Canopy Model |
| UHeatEx | Urban Heat Exposure Index |
| UHI | Urban Heat Island |
| USGS | United States Geological Survey |
| USP | Urban Surface Properties |
| UTC | Coordinated Universal Time |
| WRF | Weather Research and Forecasting Model |
| WUDAPT | World Urban Database and Access Portal Tools |

## References


1. Stewart, I.D.; Oke, T.R. Local climate zones for urban temperature studies. *Bull. Am. Meteorol. Soc.* **2012**, *93*, 1879–1900. [CrossRef]
2. Oke, T.R. The energetic basis of the urban heat island. *Q. J. R. Meteorol. Soc.* **1982**, *108*, 1–24. [CrossRef]
3. Zhou, B.; Rybski, D.; Kropp, J.P. The role of city size and urban form in the surface urban heat island. *Sci. Rep.* **2017**, *7*, 4791. [CrossRef]
4. Oke, T.R.; Johnson, G.T.; Steyn, D.G.; Watson, I.D. Simulation of surface urban heat islands under 'ideal' conditions at night part 2: Diagnosis of causation. *Bound.-Layer Meteorol.* **1991**, *56*, 339–358. [CrossRef]
5. Santamouris, M. Cooling the cities—A review of reflective and green roof mitigation technologies to fight heat island and improve comfort in urban environments. *Sol. Energy* **2014**, *103*, 682–703. [CrossRef]
6. Lhotka, O.; Kyselý, J.; Plavcová, E. Evaluation of major heat waves' mechanisms in EURO-CORDEX RCMs over Central Europe. *Clim. Dyn.* **2018**, *50*, 4249–4262. [CrossRef]
7. Founda, D.; Santamouris, M. Synergies between Urban Heat Island and Heat Waves in Athens (Greece), during an extremely hot summer (2012). *Sci. Rep.* **2017**, *7*, 10973. [CrossRef]
8. Luber, G.; McGeehin, M. Climate change and extreme heat events. *Am. J. Prev. Med.* **2008**, *35*, 429–435. [CrossRef] [PubMed]
9. Li, D.; Bou-Zeid, E. Synergistic interactions between urban heat islands and heat waves: The impact in cities is larger than the sum of its parts. *J. Appl. Meteorol. Climatol.* **2013**, *52*, 2051–2064. [CrossRef]
10. Mathieu, R.; Freeman, C.; Aryal, J. Mapping private gardens in urban areas using object-oriented techniques and very high-resolution satellite imagery. *Landsc. Urban Plan.* **2007**, *81*, 179–192. [CrossRef]
11. Smith, C. *London: Garden City? Investigating the Changing Anatomy of London's Private Gardens, and the Scale of Their Loss*; London Wildlife Trust; Greenspace Information Greater London; Greater London Authority: London, UK, 2010.
12. Ayata, T.; Tabares-Velasco, P.C.; Srebric, J. An investigation of sensible heat fluxes at a green roof in a laboratory setup. *Build. Environ.* **2011**, *46*, 1851–1861. [CrossRef]
13. Dudorova, N.V.; Belan, B.D. The Energy Model of Urban Heat Island. *Atmosphere* **2022**, *13*, 457. [CrossRef]
14. Sharma, A.; Conry, P.; Fernando, H.J.S.; Hamlet, A.F.; Hellmann, J.J.; Chen, F. Green and cool roofs to mitigate urban heat island effects in the Chicago metropolitan area: Evaluation with a regional climate model. *Environ. Res. Lett.* **2016**, *11*, 064004. [CrossRef]
15. Theodosiou, T. Green roofs in buildings: Thermal and environmental behaviour. *Adv. Build. Energy Res.* **2009**, *3*, 271–288. [CrossRef]
16. Li, X.X.; Norford, L.K. Evaluation of cool roof and vegetations in mitigating urban heat island in a tropical city, Singapore. *Urban Clim.* **2016**, *16*, 59–74. [CrossRef]
17. Porcaro, M. Potential of Energy Demand Reduction in Buildings with Green Roofs Under Climatic Conditions of Southern Europe. Ph.D. Thesis, University of Cordoba, Cordoba, Spain, May 2021.

18. Sailor, D.J.; Elley, T.B.; Gibson, M. Exploring the building energy impacts of green roof design decisions—A modeling study of buildings in four distinct climates. *J. Build. Phys.* **2011**, *35*, 372–391. [CrossRef]
19. Yoshida, A.; Hisabayashi, T.; Kashihara, K.; Kinoshita, S.; Hashida, S. Evaluation of effect of tree canopy on thermal environment, thermal sensation, and mental state. *Urban Clim.* **2015**, *14*, 240–250. [CrossRef]
20. Zhang, N.; Chen, Y.; Luo, L.; Wang, Y. Effectiveness of different urban heat island mitigation methods and their regional impacts. *J. Hydrometeorol.* **2017**, *18*, 2991–3012. [CrossRef]
21. Imran, H.M.; Kala, J.; Ng, A.W.M.; Muthukumaran, S. Effectiveness of green and cool roofs in mitigating urban heat island effects during a heatwave event in the city of Melbourne in southeast Australia. *J. Clean. Prod.* **2018**, *197*, 393–405. [CrossRef]
22. Morakinyo, T.E.; Dahanayake, K.K.C.; Ng, E.; Chow, C.L. Temperature and cooling demand reduction by green-roof types in different climates and urban densities: A co-simulation parametric study. *Energy Build.* **2017**, *145*, 226–237. [CrossRef]
23. Georgescu, M.; Morefield, P.E.; Bierwagen, B.G.; Weaver, C.P. Urban adaptation can roll back warming of emerging megapolitan regions. *Proc. Natl. Acad. Sci. USA* **2014**, *111*, 2909–2914. [CrossRef] [PubMed]
24. Jamei, E.; Chau, H.W.; Seyedmahmoudian, M.; Stojcevski, A. Review on the cooling potential of green roofs in different climates. *Sci. Total Environ.* **2021**, *791*, 148407. [CrossRef] [PubMed]
25. Rafael, S.; Correia, L.P.; Ascenso, A.; Augusto, B.; Lopes, D.; Miranda, A.I. Are green roofs the path to clean air and low carbon cities? *Sci. Total Environ.* **2021**, *798*, 149313. [CrossRef] [PubMed]
26. Voogt, J.A. *Urban Heat Islands: Hotter Cities*; America Institute of Biological Sciences: Herndon, VA, USA, 2004; pp. 4–7.
27. University Corporation for Atmospheric Research. Urban Heat Islands. 2011. Available online: https://scied.ucar.edu/longcontent/urban-heat-islands (accessed on 3 November 2024).
28. Agathangelidis, I.; Cartalis, C.; Santamouris, M. Integrating urban form, function, and energy fluxes in a heat exposure indicator in view of intra-urban Heat Island assessment and climate change adaptation. *Climate* **2019**, *7*, 75. [CrossRef]
29. Mihalakakou, G.; Souliotis, M.; Papadaki, M.; Menounou, P.; Dimopoulos, P.; Kolokotsa, D.; Paravantis, J.A.; Tsangrassoulis, A.; Panaras, G.; Giannakopoulos, E.; et al. Green roofs as a nature-based solution for improving urban sustainability: Progress and perspectives. *Renew. Sustain. Energy Rev.* **2023**, *180*, 113306. [CrossRef]
30. Tseliou, A.; Melas, E.; Mela, A.; Tsiros, I.; Zervas, E. The Effect of Green Roofs and Green Façades in the Pedestrian Thermal Comfort of a Mediterranean Urban Residential Area. *Atmosphere* **2023**, *14*, 1512. [CrossRef]
31. Iaria, J.; Susca, T. Analytic Hierarchy Processes (AHP) evaluation of green roof-and green wall-based UHI mitigation strategies via ENVI-met simulations. *Urban Clim.* **2022**, *46*, 101293. [CrossRef]
32. Scolaro, T.P.; Ghisi, E.; Silva, C.M. Assessing the impact of evapotranspiration from green roofs on reducing surface temperatures. *J. Build. Eng.* **2024**, *95*, 110095. [CrossRef]
33. Göç Yener, Ü. Green Roof as an Element of Green Infrastructure and Inferences for Implementations in Turkey. Master's Thesis, Middle East Technical University, Ankara, Türkiye, 2021.
34. Zhao, L.; Oppenheimer, M.; Zhu, Q.; Baldwin, J.W.; Ebi, K.L.; Bou-Zeid, E.; Guan, K.; Liu, X. Interactions between urban heat islands and heat waves. *Environ. Res. Lett.* **2018**, *13*, 034003. [CrossRef]
35. Dimitriadou, L.; Zerefos, C. Heatwaves and Mortality in Spain and Greece: A Comparative Analysis. *Atmosphere* **2023**, *14*, 766. [CrossRef]
36. Pantavou, K.; Kotroni, V.; Kyros, G.; Lagouvardos, K. Thermal bioclimate in Greece based on the Universal Thermal Climate Index (UTCI) and insights into 2021 and 2023 heatwaves. *Theor. Appl. Climatol.* **2024**, *155*, 6661–6675. [CrossRef]
37. Guerreiro, S.B.; Dawson, R.J.; Kilsby, C.; Lewis, E.; Ford, A. Future heat-waves, droughts and floods in 571 European cities. *Environ. Res. Lett.* **2018**, *13*, 034009. [CrossRef]
38. Smid, M.; Russo, S.; Costa, A.C.; Granell, C.; Pebesma, E. Ranking European capitals by exposure to heat waves and cold waves. *Urban Clim.* **2009**, *27*, 388–402. [CrossRef]
39. Founda, D. Urban thermal risk. *Atmosphere* **2021**, *12*, 466. [CrossRef]
40. Dandou, A.; Papangelis, G.; Kontos, T.; Santamouris, M.; Tombrou, M. On the cooling potential of urban heating mitigation technologies in a coastal temperate city. *Landsc. Urban Plan.* **2021**, *212*, 104106. [CrossRef]
41. Martilli, A.; Clappier, A.; Rotach, M.W. An urban surface exchange parameterisation for mesoscale models. *Bound.-Layer Meteorol.* **2002**, *104*, 261–304. [CrossRef]
42. Salamanca, F.; Krpo, A.; Martilli, A.; Clappier, A. A new building energy model coupled with an urban canopy parameterization for urban climate simulations—Part I. formulation, verification, and sensitivity analysis of the model. *Theor. Appl. Climatol.* **2010**, *99*, 331–344. [CrossRef]
43. Giovannini, L.; Zardi, D.; De Franceschi, M.; Chen, F. Numerical simulations of boundary-layer processes and urban-induced alterations in an Alpine valley. *Int. J. Climatol.* **2014**, *34*, 1111–1131. [CrossRef]
44. Salamanca, F.; Zhang, Y.; Barlage, M.; Chen, F.; Mahalov, A.; Miao, S. Evaluation of the WRF-urban modeling system coupled to Noah and Noah-MP land surface models over a semiarid urban environment. *J. Geophys. Res. Atmos.* **2018**, *123*, 2387–2408. [CrossRef]
45. Zonato, A.; Martilli, A.; Gutierrez, E.; Chen, F.; He, C.; Barlage, M.; Zardi, D.; Giovannini, L. Exploring the effects of rooftop mitigation strategies on urban temperatures and energy consumption. *J. Geophys. Res. Atmos.* **2021**, *126*, e2021JD035002. [CrossRef]

46. Pappaccogli, G.; Giovannini, L.; Zardi, D.; Martilli, A. Assessing the Ability of WRF-BEP+ BEM in Reproducing the Wintertime Building Energy Consumption of an Italian Alpine City. *J. Geophys. Res. Atmos.* **2021**, *126*, e2020JD033652. [CrossRef]
47. Giannaros, C.; Nenes, A.; Giannaros, T.M.; Kourtidis, K.; Melas, D. A comprehensive approach for the simulation of the Urban Heat Island effect with the WRF/SLUCM modeling system: The case of Athens (Greece). *Atmos. Res.* **2018**, *201*, 86–101. [CrossRef]
48. Ribeiro, I.; Martilli, A.; Falls, M.; Zonato, A.; Villalba, G. Highly resolved WRF-BEP/BEM simulations over Barcelona urban area with LCZ. *Atmos. Res.* **2021**, *248*, 105220. [CrossRef]
49. Zonato, A.; Martilli, A.; Di Sabatino, S.; Zardi, D.; Giovannini, L. Evaluating the performance of a novel WUDAPT averaging technique to define urban morphology with mesoscale models. *Urban Clim.* **2020**, *31*, 100584. [CrossRef]
50. Molnár, G.; Gyöngyösi, A.Z.; Gál, T. Integration of an LCZ-based classification into WRF to assess the intra-urban temperature pattern under a heatwave period in Szeged, Hungary. *Theor. Appl. Climatol.* **2019**, *138*, 1139–1158. [CrossRef]
51. Hammerberg, K.; Brousse, O.; Martilli, A.; Mahdavi, A. Implications of employing detailed urban canopy parameters for mesoscale climate modelling: A comparison between WUDAPT and GIS databases over Vienna, Austria. *Int. J. Climatol.* **2018**, *38*, e1241–e1257. [CrossRef]
52. Giannaros, C.; Agathangelidis, I.; Papavasileiou, G.; Galanaki, E.; Kotroni, V.; Lagouvardos, K.; Giannaros, T.M.; Cartalis, C.; Matzarakis, A. The extreme heat wave of July–August 2021 in the Athens urban area (Greece): Atmospheric and human-biometeorological analysis exploiting ultra-high resolution numerical modeling and the local climate zone framework. *Sci. Total Environ.* **2023**, *857*, 159300. [CrossRef]
53. Dandou, A.; Tombrou, M.; Soulakellis, N. The Influence of the City of Athens on the Evolution of the Sea-Breeze Front. *Bound.-Layer Meteorol.* **2009**, *131*, 35–51. [CrossRef]
54. Tombrou, M.; Bossioli, E.; Kalogiros, J.; Allan, J.D.; Bacak, A.; Biskos, G.; Coe, H.; Dandou, A.; Kouvarakis, G.; Mihalopoulos, N.; et al. Physical and chemical processes of air masses in the Aegean Sea during Etesians: Aegean-GAME airborne campaign. *Sci. Total Environ.* **2015**, *506*, 201–216. [CrossRef]
55. Founda, D.; Mamara, A.; Argiriou, A.; Pierros, F.; Sarantopoulos, A. Spatial and Temporal Changes of Diurnal Temperature Range in Greece—The Urban Effect. *Environ. Sci. Proc.* **2023**, *26*, 1. [CrossRef]
56. Founda, D.; Katavoutas, G.; Pierros, F.; Mihalopoulos, N. The Extreme Heat Wave of Summer 2021 in Athens (Greece): Cumulative Heat and Exposure to Heat Stress. *Sustainability* **2022**, *14*, 7766. [CrossRef]
57. Getter, K.L.; Rowe, D.B. The role of extensive green roofs in sustainable development. *HortScience* **2006**, *41*, 1276–1285. [CrossRef]
58. Carter, T.; Butler, C. Ecological impacts of replacing traditional roofs with green roofs in two urban areas. *Cities Environ. CATE* **2008**, *1*, 9. Available online: https://digitalcommons.lmu.edu/cate/vol1/iss2/9 (accessed on 3 November 2024).
59. Durhman, A.K.; Rowe, D.B.; Rugh, C.L. Effect of watering regimen on chlorophyll fluorescence and growth of selected green roof plant taxa. *HortScience* **2006**, *41*, 1623–1628. [CrossRef]
60. De Munck, C.S.; Lemonsu, A.; Bouzouidja, R.; Masson, V.; Claverie, R. The GREENROOF module (v7. 3) for modelling green roof hydrological and energetic performances within TEB. *Geosci. Model Dev.* **2013**, *6*, 1941–1960. [CrossRef]
61. Masson, V.; Champeaux, J.; Chauvin, F.; Meriguet, C.; Lacaze, R. A Global Database of Land Surface Parameters at 1-km Resolution in Meteorological and Climate Models. *J. Clim.* **2003**, *16*, 1261–1282. [CrossRef]
62. Skamarock, W.C.; Klemp, J.B.; Dudhia, J.; Gill, D.O.; Liu, Z.; Berner, J.; Wang, W.; Powers, J.G.; Duda, M.G.; Barker, D.M.; et al. *A Description of the Advanced Research WRF Model Version 4*; National Center for Atmospheric Research: Boulder, CO, USA, 2019.
63. Zhu, D.; Ooka, R. WRF-based scenario experiment research on urban heat island: A review. *Urban Clim.* **2023**, *49*, 101512. [CrossRef]
64. Demuzere, M.; Argüeso, D.; Zonato, A.; Kittner, J. W2W: A Python package that injects WUDAPT's Local Climate Zone information in WRF. *J. Open Source Softw.* **2022**, *7*, 4432. [CrossRef]
65. Mitchel, A. *The ESRI Guide to GIS Analysis, Volume 2: Spartial Measurements and Statistics*; ESRI Press: Redlands, CA, USA, 2005.
66. Janjic, Z.I.; Gerrity, J.P.; Nickovic, S. An alternative approach to nonhydrostatic modeling. *Mon. Weather Rev.* **2001**, *129*, 1164–1178. [CrossRef]
67. Monin, A.S.; Obukhov, A.M. Basic Laws of Turbulent Mixing in the Surface Layer of the Atmosphere. *Contrib. Geophys. Inst. Acad. Sci. USSR* **1954**, *24*, 163–187.
68. Janjić, Z.I. The step-mountain eta coordinate model: Further developments of the convection, viscous sublayer, and turbulence closure schemes. *Mon. Weather Rev.* **1994**, *122*, 927–945. [CrossRef]
69. Iacono, M.J.; Mlawer, E.J.; Clough, S.A.; Morcrette, J.J. Impact of an improved longwave radiation model, RRTM, on the energy budget and thermodynamic properties of the NCAR community climate model, CCM3. *J. Geophys. Res. Atmos.* **2000**, *105*, 14873–14890. [CrossRef]
70. Liang, T.; He, J.; Chen, L.; Yao, Z.; Zhang, L.; Che, H.; Gong, S. Simulation of the influence of a fine-scale urban underlying surface on the urban heat island effect in Beijing. *Atmos. Res.* **2021**, *262*, 105786. [CrossRef]
71. Zhao, L.; Lee, X.; Smith, R.B.; Oleson, K. Strong contributions of local background climate to urban heat islands. *Nature* **2014**, *511*, 216–219. [CrossRef]


**Disclaimer/Publisher's Note:** The statements, opinions and data contained in all publications are solely those of the individual author(s) and contributor(s) and not of MDPI and/or the editor(s). MDPI and/or the editor(s) disclaim responsibility for any injury to people or property resulting from any ideas, methods, instructions or products referred to in the content.